

Additive manufacturing of silicon nitride ceramics: A review of advances and perspectives

Xingjie Dong^{1,2} | Jianqin Wu^{1,2} | Honglin Yu³ | Qing Zhou^{1,2} | Wenqing Wang^{1,2} |
 Xueqin Zhang^{1,2} | Lu Zhang^{1,2} | Ling Li³ | Rujie He^{1,2}

¹State Key Laboratory of Explosion Science and Technology, Beijing Institute of Technology, Beijing, China

²Institute of Advanced Structure Technology, Beijing Institute of Technology, Beijing, China

³Shandong Industrial Ceramics Research & Design Institute Co. Ltd., Zibo, China

Correspondence

Ling Li, Shandong Industrial Ceramics Research & Design Institute Co. Ltd., Zibo 255000, China.
 Email: sinomaliling@126.com

Rujie He, State Key Laboratory of Explosion Science and Technology, Beijing Institute of Technology, Beijing 100081, China.
 Email: herujie@bit.edu.cn

Funding information

National Natural Science Foundation of China, Grant/Award Numbers: 51772028, 91960102; Open Project of State Key Laboratory of Explosion Science and Technology, Grant/Award Number: QNKT22-15

Abstract

Silicon nitride (Si_3N_4) ceramic has been widely applied in various engineering fields. The emergence of additive manufacturing (AM) technologies provides an innovative approach for the fabrication of complex-shaped Si_3N_4 ceramic components. This article systematically reviews the advances of the AM of Si_3N_4 ceramic in recent years and forecasts the potential perspectives in this field. This review aims to motivate future research and development for the AM of Si_3N_4 ceramic.

KEY WORDS

additive manufacturing, ceramic, silicon nitride

1 | INTRODUCTION

Silicon nitride (Si_3N_4) ceramic has been widely applied in military, mechanical engineering, aerospace, and biomedical fields, such as missile radomes,¹ rocket nozzles,² turbine and automotive engine components,³ tool bits,⁴ wear-resistant bearings, hip or knee endoprosthetic implants, and dental implants,⁵ owing to its promising combined properties of excellent mechanical properties, thermal shock resistance at elevated temperatures, good dielectric properties and biocompatibility^{6–10} (as shown in Figure 1). At present, the demand for high-performance complex-shaped Si_3N_4 ceramic components in different applications is increasingly urgent, which has attracted the interest of many researchers.

Since 1950s, the increasing demand for the use of Si_3N_4 ceramic has led to the continuous development of its manufacture methods.^{11,12} Initially, the traditional fabrication of Si_3N_4 ceramic includes dry pressing combined with pressureless sintering^{13,14} or hot-pressing sintering,^{15,16} and cold isostatic pressing (CIP) followed by gas pressure sintering,^{17–19} and so on. Although Si_3N_4 ceramic prepared by these conventional technologies have high density and good mechanical properties, they generally require a post-machining treatment (such as grinding, cutting, and machining²⁰), which is both expensive and difficult due to various high-cost machining tools and the inherent brittleness of ceramic. Subsequently, many traditional near-net-shape fabrication methods begin to appear for Si_3N_4 ceramic, such as injection molding^{21,22}

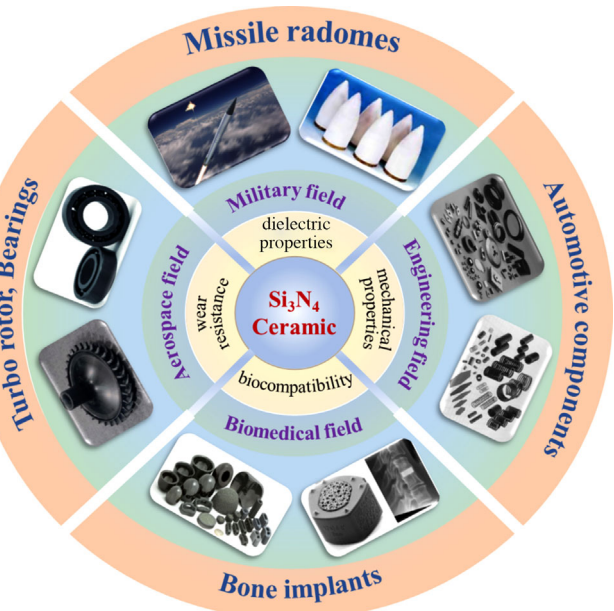


FIGURE 1 Properties and applications of Si_3N_4 ceramic

and gel-casting.^{23,24} These methods are usually combined with pressureless sintering to produce Si_3N_4 ceramic parts, which avoid the trouble of post-mechanical processing to a certain extent. However, the need for molds still makes these methods time-wasting and limited for producing high-complex-shaped Si_3N_4 ceramic components. Therefore, novel advanced manufacturing technologies for Si_3N_4 ceramic are deemed necessary to develop.

Additive manufacturing (AM), also known as 3D printing (3DP) or solid freeform fabrication, refers to the process of combining materials to fabricate components from 3D models layer-by-layer. AM has attracted great attentions due to its obvious advantages in recent years. Apart from the enormous time and cost savings, AM has part and production flexibility. Because there are no tooling constraints, parts with complex shapes can be made in a single piece.²⁵ Moreover, the more complicated a product's structure is, the more clear the benefits of AM become. Therefore, the emergence of AM technologies provides an innovative technological approach for the fabrication of complex-shaped ceramics. Currently, typical oxide ceramics (such as Al_2O_3 ,^{26,27} ZrO_2 ,^{28–30} etc.), precursor-derived ceramics (such as SiOC ,^{31,32} SiCN ,^{33,34} etc.), bio-ceramics (such as hydroxyapatite,^{35,36} calcium phosphate,^{37,38} etc.), and even some ceramic matrix composites (such as $\text{SiC}_w/\text{Al}_2\text{O}_3$,^{39,40} C_{sf}/SiC ,^{41,42} etc.) have been successfully prepared by using various AM technologies. However, compared to other ceramic materials, Si_3N_4 ceramics have a high refractive index, which will lead to difficulties in forming during the photopolymerization AM process. Besides, its strong covalent bonding can

also lead to difficulties in densification after AM. Therefore, till now, there have been relatively few reports on AM of Si_3N_4 ceramic.

Fortunately, the research on the AM of Si_3N_4 ceramic has received more and more attentions recently, and attempts have been on the rise. AM technologies of Si_3N_4 ceramics mainly include (1) powder bed fusion (including selective laser sintering [SLS], and selective laser melting [SLM],^{43–49} and so on), (2) photopolymerization (usually including stereolithography apparatus [SLA],⁵⁰ laser-induced slip [LIS] casting,⁵¹ digital light processing [DLP],^{52–65} liquid crystal display [LCD],^{66,67} and so on); (3) material extrusion (usually including direct ink writing [DIW] or robocasting,^{68–74} fused deposition modeling [FDM],^{75–79} and so on); and (4) other AM technologies (including binder jetting [BJ],^{80–85} 3DP,^{86–89} and laminated object manufacturing [LOM]^{90–94}). Schematics of the previous AM technologies for Si_3N_4 ceramic are illustrated in Figure 2.

Here, therefore, we aim to summarize the advances of AM of Si_3N_4 ceramic as systematically and comprehensively as possible and forecast future potential perspectives. In this review, the advances of AM technologies of Si_3N_4 ceramic will be described in Section 2, and the perspectives will be introduced in Section 3. The authors hope that this review will provide a deep insight into the AM of Si_3N_4 ceramic.

2 | ADVANCES

2.1 | Powder bed fusion

Powder bed fusion technology mainly includes SLS and SLM. They create 3D parts through the application of laser energy to powder beds via the CAD description of the part geometry, as shown in Figure 2A. The difference between SLS and SLM is that the temperature at which the laser irradiates the powder is higher or lower than the melting point of the powder. The advantage of SLS/SLM is that there are many materials they can use, including polymers, metals, ceramics, gypsum, nylon, and other powders. However, the main drawback of SLS/SLM techniques is the residual stresses from rapid heating followed by the solidification during the manufacturing, which could introduce cracks or even entire structural failure.⁹⁵

SLS/SLM of Si_3N_4 ceramic is extremely challenging due to poor sinterability caused by the low absorption of laser beam energy. Therefore, Minasyan et al.⁴³ proposed an indirect approach to fabricate Si_3N_4 -based ceramic parts with complex geometry by SLS. First, SLS of silicon powder provided a needed shape, and then the nitridation of the as-shaped silicon parts aimed at the fabrication of Si_3N_4

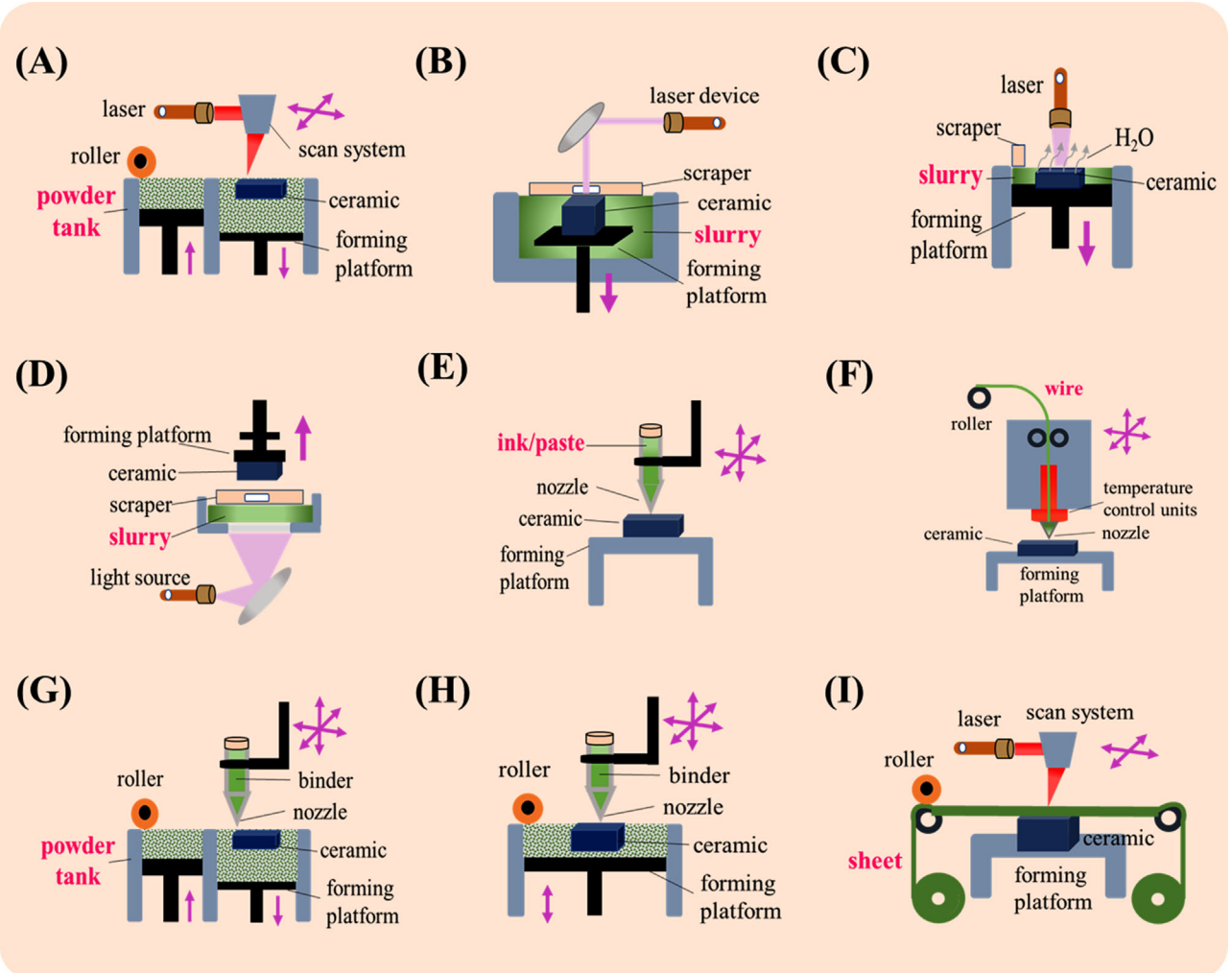


FIGURE 2 Schematics of additive manufacturing (AM) technologies for Si_3N_4 ceramic: (A) selective laser sintering (SLS)/selective laser melting (SLM); (B) stereolithography apparatus (SLA); (C) laser-induced slip (LIS); (D) digital light processing (DLP), liquid crystal display (LCD); (E) direct ink writing (DIW) (robocasting); (F) fused deposition modeling (FDM); (G) binder jetting (BJ); (H) 3D printing (3DP); (I) laminated object manufacturing (LOM).

ceramic component. They investigated the influences of laser current, point distance, and exposure time on the morphology, density, and mechanical properties of the sintered Si_3N_4 ceramic samples. The result showed that the SLS-3D printed Si parts reached a geometrical density of 82%, a Vickers hardness of 11.8 GPa, and a compressive strength of 432 MPa, respectively. In their further work,⁴⁴ core-shell-structured $\text{MoSi}_2/(10\text{--}13 \text{ wt.\%})\text{Si}$ powders were used for the fabrication of $\text{MoSi}_2/\text{Si}_3\text{N}_4$ cellular mesostructures by the same indirect method, as shown in Figure 3A (reproduced with permission from Ref. [44] 2019 Elsevier). The silicon shell of core-shell-structured MoSi_2/Si powder served as a binder phase that provided the relevant laser absorption, whereas the MoSi_2 core provided the mechanical durability. Although their work transformed MoSi_2/Si lattices into $\text{MoSi}_2\text{--}\text{Si}_3\text{N}_4$ ceramic composites, the theoretical amounts of Si_3N_4 after nitridation were

not high enough, resulting in poor mechanical properties. Moreover, the indirect SLS/SLM method is usually cumbersome and time-consuming. Wei et al.⁴⁵ directly fabricated a pre-sintered Si_3N_4 ceramic with a porosity of 80% by SLS in the air atmosphere. They found that the bonding of the SLS-3D printed Si_3N_4 ceramic depended on microvilli and nanowires on its surface, which is shown in Figure 3B (reproduced with permission from Ref. [45] 2019 Elsevier). This bonding mechanism was significantly different from that of metals or oxide ceramics.^{96,97} Although they directly manufactured porous Si_3N_4 ceramic by SLS, the mechanical properties of the as-prepared porous Si_3N_4 ceramic were poor and could only satisfy the following posttreatment requirements. Therefore, Wang et al.⁴⁶ attempted to fabricate high-strength Si_3N_4 ceramic antenna windows via SLS with CIP after debinding before final sintering. The strength of the SLS-3D printed Si_3N_4

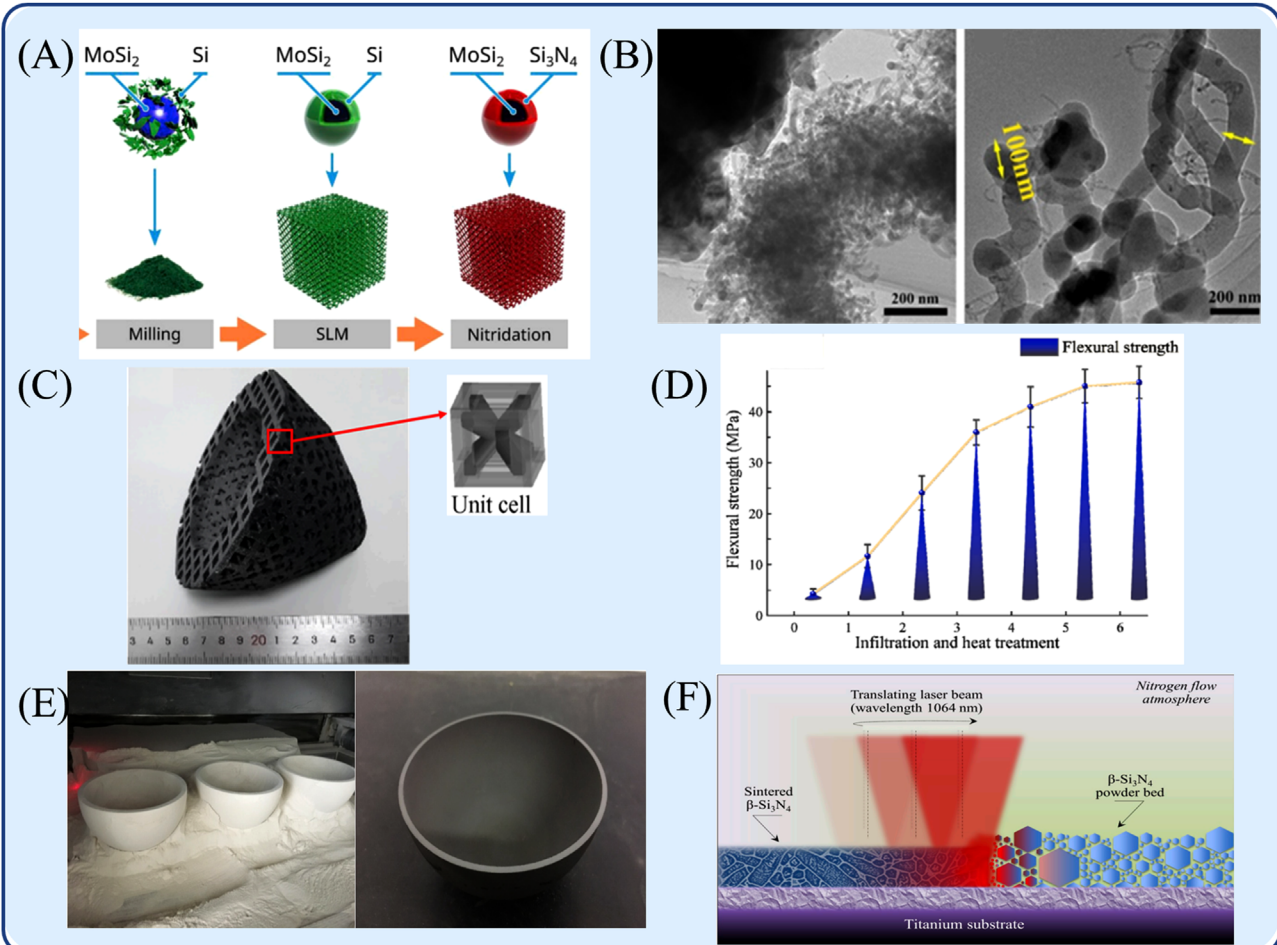


FIGURE 3 (A) Selective laser melting (SLM) fabrication procedure for $\text{MoSi}_2\text{-Si}_3\text{N}_4$ ceramic lattice, (B) bonding mechanism of Si_3N_4 ceramic depended on microvilli and nanowire on its surface, (C) $\text{Si}_3\text{N}_4\text{-SiC}/\text{SiO}_2$ composite part fabricated by selective laser sintering (SLS) and sol infiltration (SI), (D) flexural strengths of the $\text{Si}_3\text{N}_4\text{-SiC}/\text{SiO}_2$ composites subjected to various infiltration and heat-treatment cycles, (E) hemispherical green bodies and sintered Si_3N_4 ceramic housing, (F) SLS fabrication procedure proposed for a dense Si_3N_4 ceramic coating on titanium substrate. *Source:* (A) Reproduced with permission from Ref. [44] 2019 Elsevier; (B) reproduced with permission from Ref. [45] 2019 Elsevier; (C) reproduced with permission from Ref. [47] 2021 Elsevier; (D) reproduced with permission from Ref. [47] 2021 Elsevier; (E) reproduced with permission from Ref. [48] 2019 MDPI; and (F) reproduced with permission from Ref. [49] 2020 Elsevier

ceramic after sintering at 1750°C without CIP was only 12 MPa. After one CIP treatment, however, the strength of the SLS-3D printed Si_3N_4 ceramic increased significantly to 225 MPa. Moreover, after two CIP treatments, the strength of the SLS-3D printed Si_3N_4 ceramic increased even more markedly to 592 MPa. The result showed that the strength of the SLS-3D printed Si_3N_4 ceramic could be greatly improved by CIP after debinding. In addition to the previous study, Yu et al.⁴⁷ prepared $\text{Si}_3\text{N}_4\text{-SiC}/\text{SiO}_2$ ceramic composites using SLS and sol infiltration (SI) processing. SLS was used to print the green ceramic body of the desired part with complex shapes. SI process increased the density and improved the mechanical properties of the resulting $\text{Si}_3\text{N}_4\text{-SiC}/\text{SiO}_2$ composites. A photograph of the $\text{Si}_3\text{N}_4\text{-SiC}/\text{SiO}_2$ composite part is shown in Figure 3C (reproduced with permission from Ref. [47] 2021 Elsevier).

After the six silica-SI and heat treatment cycles, the flexural strength of the $\text{Si}_3\text{N}_4\text{-SiC}/\text{SiO}_2$ composite reached 42.4 MPa, which is much higher than that obtained without infiltration (as shown in Figure 3D (reproduced with permission from Ref. [47] 2021 Elsevier)). Therefore, Both CIP and SI treatment after SLS are helpful to improve the mechanical properties of the Si_3N_4 ceramic.

There are also some reports on the functional application of the SLS-3D printed Si_3N_4 ceramic. Qi et al.⁴⁸ successfully prepared gradually thickened hemispherical Si_3N_4 ceramic housings based on SLS. The printed hemispherical green bodies and the sintered Si_3N_4 ceramic housing are shown in Figure 3E (reproduced with permission from Ref. [48] 2019 MDPI). They expected to utilize SLS to achieve batch production of deep-sea pressure-resistant floatation spheres with Si_3N_4 ceramic material.

Zanocco et al.⁴⁹ produced a dense Si_3N_4 ceramic coating on a biomedical grade commercially pure titanium (cp-Ti) substrate by SLS, as shown in Figure 3F (reproduced with permission from Ref. [49] 2020 Elsevier). This technology may achieve rapid osseous fixation while resisting bacteria. The dual benefits of an Si_3N_4 ceramic coating are related to its RNS surface chemistry and slowed kinetics that favor osseointegration while inhibiting bacteria. This study had reference significance for the research of additively manufactured Si_3N_4 ceramics in the field of biomedicine.

2.2 | Photopolymerization

As the earliest form of AM, photopolymerization technology fabricates 3D parts by selectively solidifying the liquid resin in ceramic slurry through a photopolymerization reaction (except LIS casting).⁹⁸ The photopolymerization technology of ceramics is one of the most promising ceramic AM technologies that have been developed in recent years due to its fast printing speed and high precision.⁹⁹ According to the principle of formation and the control system, photopolymerization can be subdivided into SLA and DLP.

2.2.1 | Stereolithography apparatus (SLA)

SLA is relatively mature and the first AM technology to appear and achieve commercial application. During SLA, the slurry is selectively cured (from point to line, from line to surface) by a point light source that comes from a laser. The platform and print parts are placed in the slurry tank. After each layer is formed, the platform is lowered a certain distance. The curing process is repeated to prepare a complete ceramic part, as shown in Figure 2B.

Xing et al.⁵⁰ fabricated an $\text{Al}_2\text{O}_3\text{-Si}_3\text{N}_4$ functionally graded material (FGM) part using SLA. They designed six groups of ceramic slurries, with an Si_3N_4 content gradient of 20 vol.%, to realize the uniform transition from Al_2O_3 to Si_3N_4 , as shown in Figure 4A (reproduced with permission from Ref. [50] 2020 Elsevier). The SLA parameters were adjusted because the contents of Si_3N_4 had significant effects on the slurries' curing performance and rheological behavior. They proposed a modified formula to evaluate the relationship between the actual minimum voidage of mixtures and the viscosities of their corresponding pastes and established a mathematical relationship between the Si_3N_4 content and the curing thickness of paste. The FGM green body was printed in a layer thickness of 40 μm through a series of optimized laser power and scanning speed parameters for each group of slurry. Finally, a dense $\text{Al}_2\text{O}_3\text{-Si}_3\text{N}_4$ gradient ceramic in complicated shape was obtained after debinding and sintering.

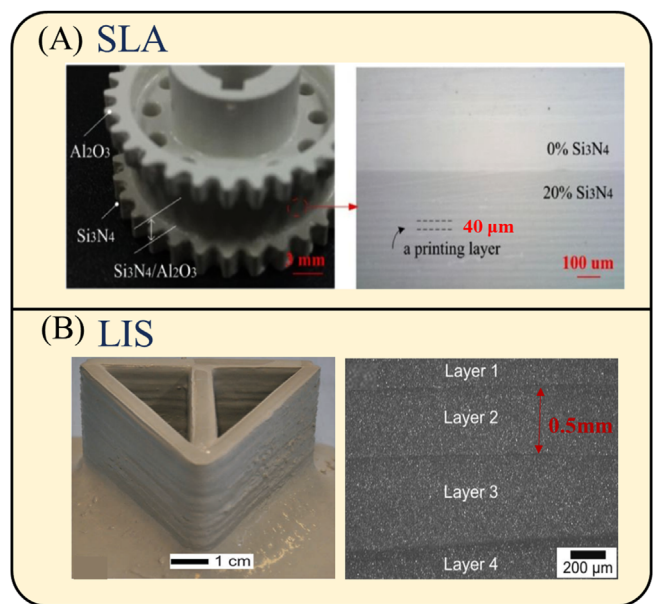


FIGURE 4 (A) Stereolithography apparatus (SLA)-3D printed $\text{Al}_2\text{O}_3\text{-Si}_3\text{N}_4$ gradient ceramic in complicated shape, (B) laser-induced slip (LIS)-3D printed Si_3N_4 green body and its cross-section microstructure. *Source:* (A) Reproduced with permission from Ref. [50] 2020 Elsevier and (B) reproduced with permission from Ref. [51] 2017 Goeller

complicated shape without macro defects was obtained after debinding and sintering. This study provided a design and fabrication strategy for multi-ceramic FGM based on SLA-3DP technology.

Like most AM processes, the printing process of LIS is a layer-by-layer process, in which the CAD data of the part to be built is written in the individual layers, as shown in Figure 2C. What is different between LIS and SLA is that the solvent of the LIS slurry is removed by local evaporation, which is achieved by intense laser radiation writing the desired geometry in a freshly deposited layer of slurry. With subsequent repetition of the steps of layer deposition and laser drying, a part is built. The advantages of LIS are that it avoids the hassle of having polymers in the slurry and enables larger cured thickness. Lüchtenborg et al.⁵¹ introduced the LIS process using Si_3N_4 slurry as an example. The process was designed to generate voluminous ceramic parts employing the layer-wise buildup of parts with a layer thickness larger than .5 mm. Si_3N_4 green body generated by the LIS process and the cross section of a green body are shown in Figure 4B (reproduced with permission from Ref. [51] 2017 Goeller). Although the microstructure of the parts produced with LIS revealed flaws like pores and delaminations, the density of Si_3N_4 ceramics after sintering had reached up to 99.4%, and the 4-point flexural strength reached up to 323 MPa.

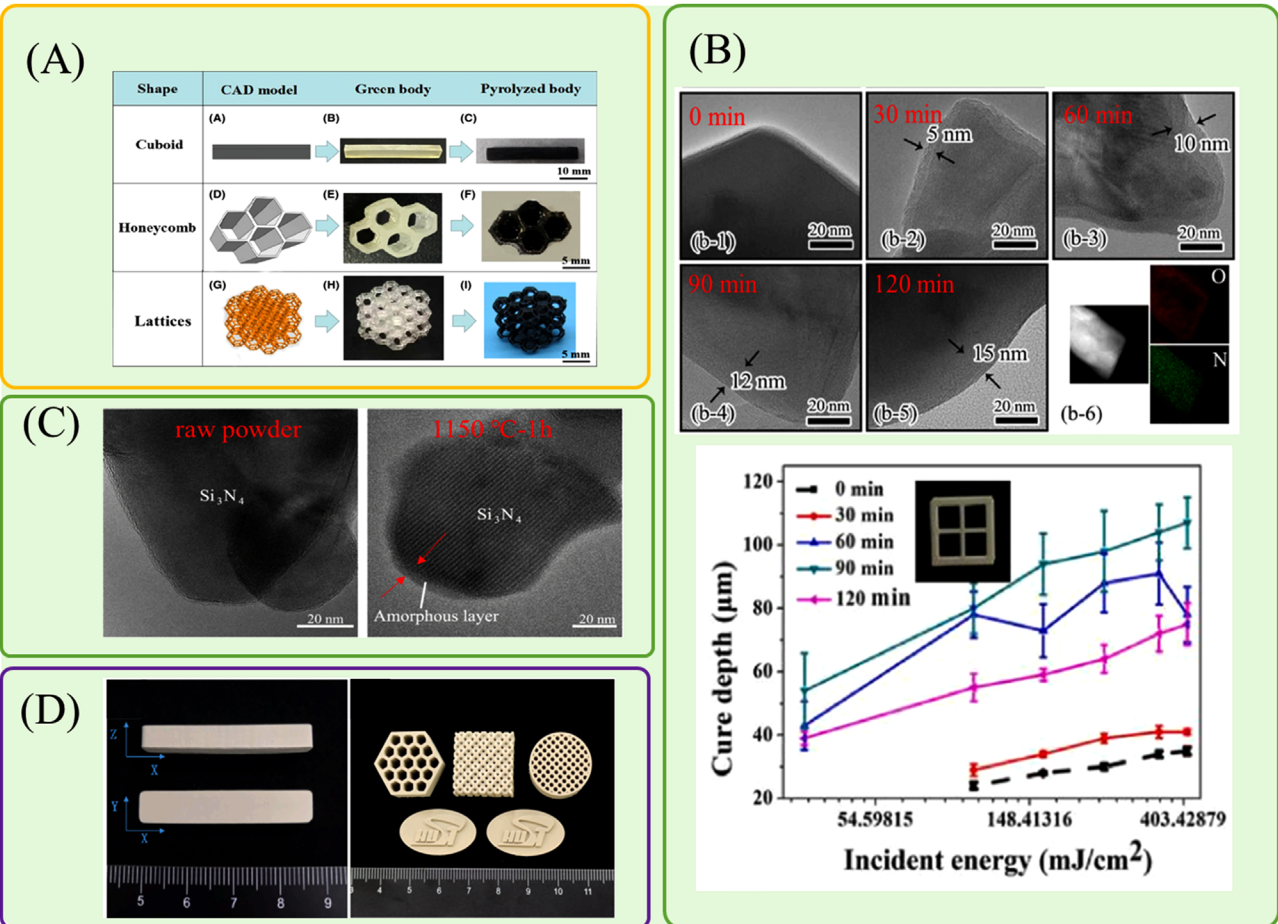


FIGURE 5 (A) Digital light processing (DLP)-3D printed Si₃N₄ ceramic cuboid, honeycomb, and lattice structures from preceramic polymers, (B) TEM images and cure depth of Si₃N₄ powders with different oxidation times, (C) TEM micrographs of raw Si₃N₄ powder and sample 1150°C-1 h, (D) DLP-3D printed Si₃N₄ ceramic part, which used Si₃N₄ powder coated with Al₂O₃-Y₂O₃ sintering additives by chemical co-precipitation method. *Source:* (A) Reproduced with permission from Ref. [52] 2019 John Wiley and Sons; (B) reproduced with permission from Ref. [54] 2022 Elsevier; (C) reproduced with permission from Ref. [55] 2019 Elsevier; (D) reproduced with permission from Ref. [59] 2022 Elsevier

2.2.2 | Digital light processing (DLP)

DLP is an AM technology developed on the basis of SLA. Its forming direction is opposite to SLA. During DLP, the slurry is selectively cured by a space light source that comes from a UV light device. Usually, the UV light device is below the slurry tank. The scraper spreads back and forth, and the platform rises and falls according to the preset program. Finally, the curing is conducted layer by layer, and a green body is obtained. The schematic diagram of the DLP process is shown in Figure 2D.

Wang et al.⁵² proposed and demonstrated, for the first time, AM of simple and complex-shaped Si₃N₄ ceramic components using DLP and pyrolysis from preceramic polymers polysilazanes. Simple Si₃N₄ ceramic cuboid, 2D-structured Si₃N₄ ceramic honeycomb, and 3D-structured Si₃N₄ ceramic lattice with high precision were fabricated

(as shown in Figure 5A (reproduced with permission from Ref. [52] 2019 John Wiley and Sons)). The 3-point flexural strength of the DLP-3D printed Si₃N₄ ceramic cuboid bars was measured to be 57.3 ± 8.7 MPa. The compressive strength values of the 2D-structured Si₃N₄ ceramic honeycomb and 3D-structured Si₃N₄ ceramic lattice were 65.5 and 5.12 MPa, respectively. Although the route of polymer-derived ceramic-based DLP is relatively easy when printing, the mechanical property of the final ceramic is relatively low owing to the relatively low density after pyrolysis. In recent years, most researchers have used ceramic slurry-based DLP to prepare high-performance Si₃N₄ ceramic. However, there are still two main difficulties with DLP-3D printed Si₃N₄ ceramic: (1) The curing thickness of the DLP-3D printed Si₃N₄ slurry was not high enough, and (2) the density of the DLP-3D printed Si₃N₄ ceramics after sintering was also not ideal.

Li et al.⁵³ studied the rheology and curability characterization of photosensitive slurries for DLP of Si_3N_4 ceramic. The study showed that the viscosity of Si_3N_4 photocurable slurries was greatly affected by ambient temperature. With the temperature increased, the viscosity decreased obviously. More importantly, they also proved that the Si_3N_4 slurry had a lower curing ability when compared with oxide ceramic slurries because of the large refractive index and absorbance of Si_3N_4 slurry. Therefore, improving the curing ability of Si_3N_4 ceramic slurry attracted extensive research. One of the solutions was to use surface oxidation to attach an amorphous SiO_2 layer to the surface of Si_3N_4 powder. Li et al.⁵⁴ modified the surface of Si_3N_4 powders through oxidation with different times (30, 60, 90, and 120 min) in order to reduce the refractive index difference between the ceramic particle surface and photosensitive resin. The reaction between Si_3N_4 and O_2 during oxidation process can be shown in the following reaction:



TEM images and curing thickness of Si_3N_4 powders with different oxidation time are shown in Figure 5B (reproduced with permission from Ref. [54] 2022 Elsevier). Compared with raw ceramic powder without any oxidation, the light absorbance of the oxidized Si_3N_4 was apparently lower and decreased as prolonging the oxidation time. The result showed that the curing thickness increased as the light absorption of ceramic powder decreasing. Huang et al.⁵⁵ also oxidized Si_3N_4 powder at different temperatures and times (1150°C-1 h, 1150°C-3 h, 1200°C-1 h, and 1200°C-1 h). TEM micrographs of raw Si_3N_4 powder and the sample 1150°C-1 h are shown in Figure 5C (reproduced with permission from Ref. [55] 2019 Elsevier). At the exposure energy of 500 mJ/cm², the curing thickness of the raw Si_3N_4 powder was 34 μm . After oxidation, the curing thicknesses of the sample 1150°C-1 h, 1150°C-3 h, 1200°C-1 h, and 1200°C-1 h increased by 8, 13, 17, and 34 μm compared to raw Si_3N_4 powder, respectively. This is because both the light absorbance and refractive index of the oxidized Si_3N_4 powder reduced. Adding surface modifiers was another way to increase the curing thickness of Si_3N_4 slurry. Liu et al.⁵⁶ prepared Si_3N_4 slurry with 45 vol.% solid loading successfully by using KH560 and Darvan as the surface modifier and the dispersant, respectively. They demonstrated that surface modification of submicro- Si_3N_4 powder could be used to improve the rheological behavior and the curing ability of Si_3N_4 slurry effectively. They also studied the effects of the silane coupling agent, which was directly used as the surface modifier and dispersant, on the rheological property, stability, wettability, and curing performance of the Si_3N_4 slurry in another paper.⁵⁷ The

result showed that the dispersion, wettability, and curing thickness of Si_3N_4 slurry were all improved by adding suitable silane coupling agents. Yang et al.⁵⁸ first oxidized the Si_3N_4 powder and then modified the oxidized powder with the silane coupling agent. The oxidation process could effectively raise the curing thickness and stability of Si_3N_4 slurry. Additionally, modification by KH560 enabled the improvement of the rheological properties and wettability of Si_3N_4 slurry. The result showed that the curing behavior and the rheological properties of Si_3N_4 slurry could be effectively enhanced by the oxidation process and silane coupling agent. In addition to oxidation treatment and surface modification of Si_3N_4 powder, Li et al.⁵⁹ put forward coating the surface of Si_3N_4 powder with $\text{Al}_2\text{O}_3\text{-Y}_2\text{O}_3$ sintering additives by chemical co-precipitation method. Finally, Si_3N_4 ceramic was successfully fabricated by DLP (as shown in Figure 5D (reproduced with permission from Ref. [59] 2022 Elsevier)). The result showed that when the content of $\text{Al}(\text{NO}_3)_3$ and $\text{Y}(\text{NO}_3)_3$ solutions was 20 ml/100 g Si_3N_4 , the curing thickness of the slurry prepared with the coated Si_3N_4 powder, which was $47.9 \pm 1.2 \mu\text{m}$, was nearly 13% higher relative to the slurry prepared with raw powder. These previous studies were all through the additional treatment of Si_3N_4 powder to improve the curing properties and rheological properties, factors such as particle inherent property (color, size), resin, dispersant, and photoinitiator could also affect the curing properties and rheological properties of Si_3N_4 slurries. Liu et al.⁶⁰ investigated the mechanism of how the powder color and particle size affected the curing ability of Si_3N_4 slurries. Zou et al.⁶¹ compared the curing behavior of different functional groups and RI of resin monomer, and the dispersion effect of three commercial dispersants was investigated systematically. Wu et al.^{66,67} also studied the influence of type and content of photosensitive resin and dispersant on Si_3N_4 slurries for LCD mask stereolithography (an AM technology similar to DLP). Cao et al.⁶² investigated the effect of initiators on the curing effect of Si_3N_4 slurries. Their findings revealed that choosing right component type and content could help improve the performance of Si_3N_4 slurries to some extent.

For the density issue of Si_3N_4 ceramic, Rao et al.⁶³ also fabricated dense Si_3N_4 ceramic by combining DLP with field-assisted sintering through using CeO_2 as sintering additive. They considered that the grain boundary slipping played a dominating role in the densification process of DLP-3D printed Si_3N_4 ceramic. During the field-assisted sintering, CeO_2 sintering additive segregated in the grain boundaries and insoluble in the Si_3N_4 grains. Finally, a dense Si_3N_4 ceramic with good mechanical properties was fabricated. Therefore, the density of Si_3N_4 ceramics after photocuring may be controlled by the content and composition of rare-earth elements.

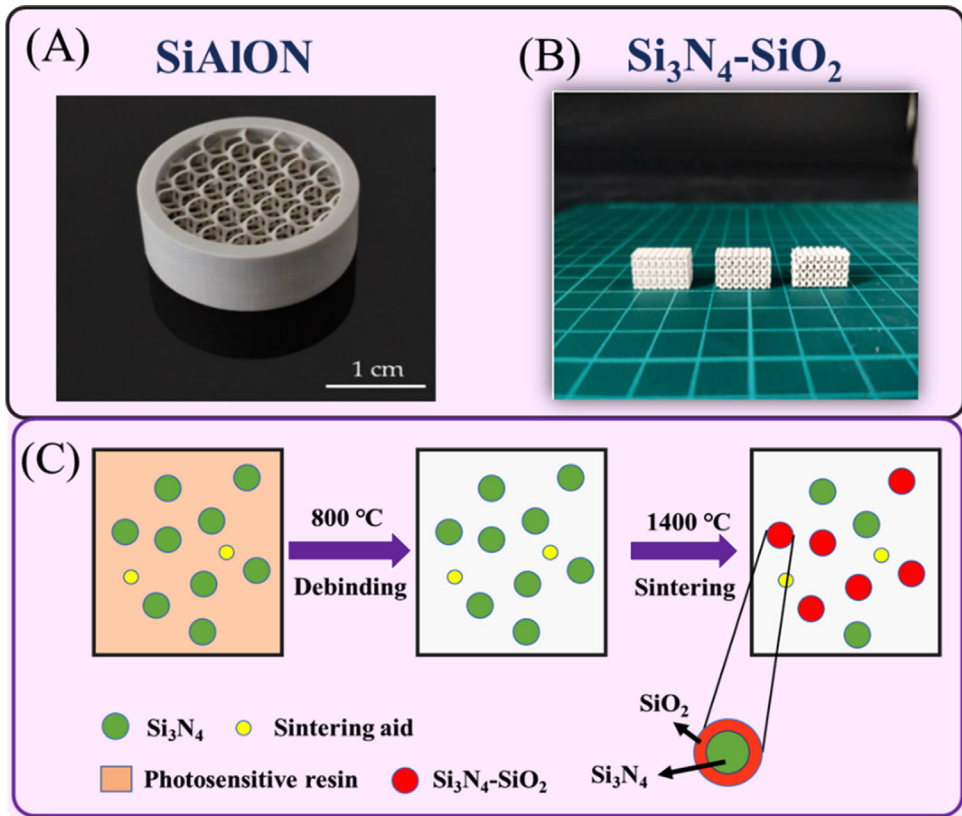


FIGURE 6 (A) Digital light processing (DLP)-3D printed SiAlON ceramic with complex architecture, (B) a broadband microwave transparent Si₃N₄-SiO₂ composite ceramic complex structures fabricated by DLP and sintering in air atmosphere, (C) the schematic synthetic reaction process of oxidation of Si₃N₄ at high temperatures. *Source:* (A) Reproduced with permission from Ref. [64] 2020 MDPI; (B) reproduced with permission from Ref. [65] 2021 Elsevier; and (C) reproduced with permission from Ref. [65] 2021 Elsevier

In addition to the previously mentioned literature, there are some reports on DLP-3D printed Si₃N₄-related materials. Altun et al.⁶⁴ manufactured a variety of Si₃N₄-based ceramic parts, SiAlON ceramics, with complex architecture by DLP (as shown in Figure 6A (reproduced with permission from Ref. [64] 2020 MDPI)). The obtained SiAlON ceramic bodies with a relative density of 99.8% exhibited a biaxial strength of 764 MPa and a hardness of 1500 (HV10). Chen et al.⁶⁵ fabricated a broadband microwave transparent complex structure Si₃N₄-SiO₂ composite with excellent performance through DLP and sintering in air atmosphere (as shown in Figure 6B (reproduced with permission from Ref. [65] 2021 Elsevier)). The strength of Si₃N₄-SiO₂ ceramic sintered at 1350°C was 77 ± 5 MPa. The relative permittivity of the as-prepared Si₃N₄-SiO₂ ceramic was within the range of less than 4, and the loss tangent could be below than .003. These results showed that the DLP-3D printed Si₃N₄-SiO₂ ceramic exhibited excellent wave-transparent performance. Besides, they also elaborated the synthetic reaction process of oxidation of Si₃N₄ at high temperatures, which is shown in Figure 6C (reproduced with permission from Ref. [65] 2021 Elsevier). This work provided a reference for the preparation

of Si₃N₄-based materials with excellent mechanical and dielectric properties by photopolymerization technology.

2.3 | Material extrusion

Material extrusion is an AM process, in which material is selectively deposited by extrusion from a nozzle. It is also an early and widely used AM technology. Material extrusion has the advantages of low cost, many applicable material systems, simple and convenient operation. According to the curing method, material extrusion can be divided into normal temperature extrusion and hot extrusion. Normal temperature extrusion mainly includes DIW or robocasting, whereas hot extrusion mainly includes FDM.

2.3.1 | Direct ink writing (DIW) or robocasting

DIW or robocasting builds 3D parts by stacking filaments layer by layer into a set route through a nozzle, as shown

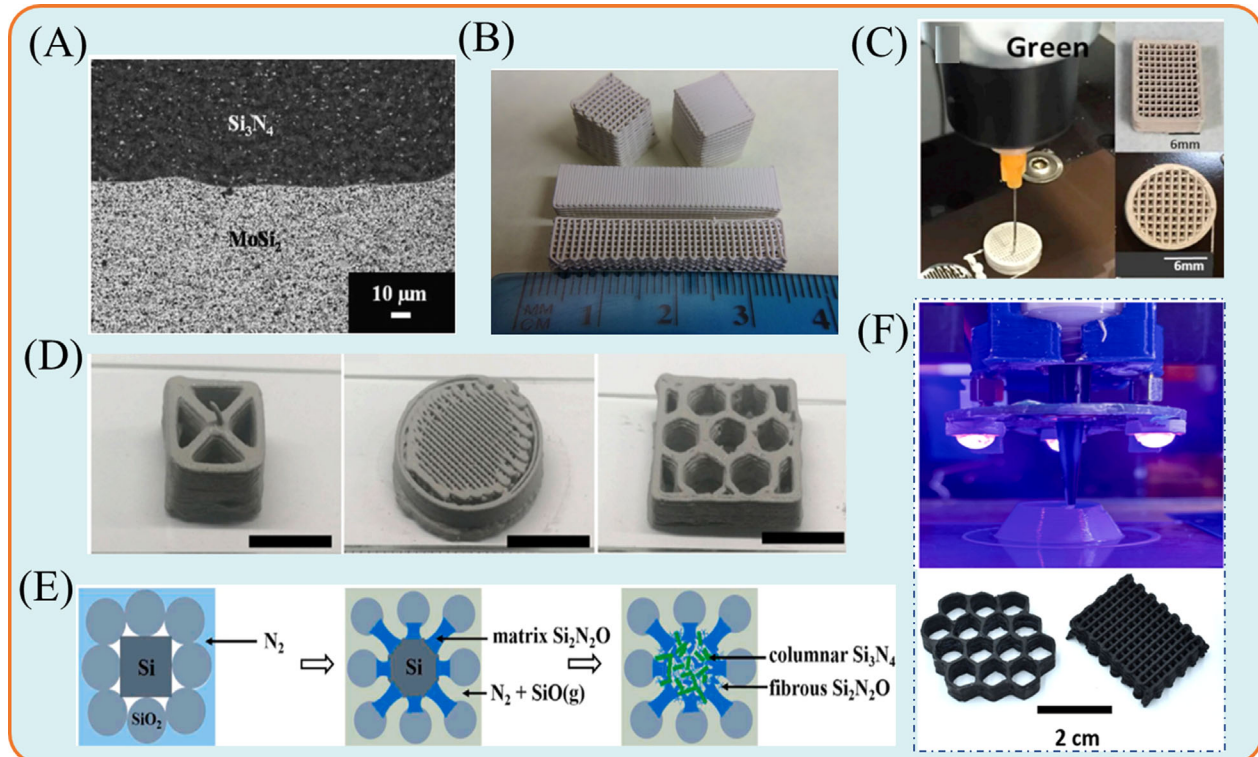


FIGURE 7 (A) Cross section of a direct ink writing (DIW)-3D printed $\text{Si}_3\text{N}_4/\text{MoSi}_2$ multilayer green sample, (B) Si_3N_4 green parts with controllable shape and architecture for biomedical applications, (C) robocasting-3D printed highly porous Si_3N_4 scaffolds with a pattern of macroporous cavities of 650–700 μm , (D) DIW-3D printed three complex-shape porous $\text{Si}_2\text{N}_2\text{O}$ ceramics strengthened by directional β - Si_3N_4 , (E) formation mechanism of $\text{Si}_2\text{N}_2\text{O}$ and Si_3N_4 at 1250°C, (F) UV-assisted DIW and the as-prepared $\text{SiC}/\text{Si}_3\text{N}_4$ composites. *Source:* (A) Reproduced with permission from Ref. [69] 2011 John Wiley and Sons; (B) reproduced with permission from Ref. [70] 2016 John Wiley and Sons; (C) reproduced with permission from Ref. [71] 2020 Elsevier; (D) reproduced with permission from Ref. [72] 2020 Elsevier; (E) reproduced with permission from Ref. [73] 2022 Elsevier; (F) reproduced with permission from Ref. [74] 2022 Elsevier

in Figure 2E. DIW employs relatively low solid loading ceramic ink as the raw material, whereas robocasting uses high solid loading ceramic paste as the raw material.¹⁰⁰ They can make parts from different materials because they have a variety of sizes of nozzles. Apart from that, their cost is relatively low. But the printing accuracy of DIW or robocasting is not high enough, which also limits their development in the preparation of Si_3N_4 ceramic components with high accuracy.

Cappi et al.⁶⁸ prepared an aqueous Si_3N_4 ink with a solid loading of 30 vol.% and manufactured high-performance complex-shaped Si_3N_4 ceramics by DIW successfully. The sintered Si_3N_4 ceramic part had a density of 3.18 g/cm³, a hardness value (HV .2) of 17, and a fracture toughness K_{IC} of 4.4 MPa m^{1/2}, respectively. In their further study,⁶⁹ they obtained dense and delamination-free Si_3N_4 and MoSi_2 samples as well as multilayer parts (as shown in Figure 7A [reproduced with permission from Ref. [69] 2011 John Wiley and Sons]) by adjusting the aqueous Si_3N_4 and MoSi_2 inks. Their study showed the high potential of DIW for producing complex-shaped non-oxide ceramics and even multifunctional parts in one process. Zhao

et al.⁷⁰ prepared Si_3N_4 ceramic with controllable shape and architecture for biomedical applications using a robocasting technique (as shown in Figure 7B (reproduced with permission from Ref. [70] 2016 John Wiley and Sons)). Two samples (including macro-porous part and solid part) were prepared after hot isostatic pressing sintering. As-fabricated solid samples in the shape of beams showed a flexural strength of 552 ± 68 MPa. Samples with a macroporous grid-like architecture (porosity = 56.5%; pore width = 350 μm) showed a flexural strength of 89 ± 11 MPa. Their research indicated that robocasting combined with hot isostatic pressing sintering provided a viable manufacturing approach to create Si_3N_4 implants with controllable shape and architecture for orthopedic and dental surgery applications. Similarly, Sainz et al.⁷¹ fabricated highly porous Si_3N_4 scaffolds by robocasting with a pattern of macroporous cavities of 650–700 μm (Figure 7C [reproduced with permission from Ref. [71] 2020 Elsevier]). The potential application of robocasting-3D printed Si_3N_4 scaffold for bone regeneration was demonstrated. In addition to the previous research reports, there are also some reports on Si_3N_4 related materials by DIW. Jin et al.⁷²

fabricated three complex-shaped porous $\text{Si}_2\text{N}_2\text{O}$ ceramics strengthened by directional $\beta\text{-Si}_3\text{N}_4$ using DIW, as shown in Figure 7D (reproduced with permission from Ref. [72] 2020 Elsevier). The mechanical properties of the as-prepared composite were greatly improved due to the addition of high-aspect-ratio $\beta\text{-Si}_3\text{N}_4$ grains. This study provided a reference for fabricating high-performance anisotropic complex-structured ceramics. Jiang et al.⁷³ prepared $\text{Si}_2\text{N}_2\text{O}\text{-Si}_3\text{N}_4$ ceramics for radome materials by DIW combined with low-temperature sintering. Strictly speaking, $\text{Si}_2\text{N}_2\text{O}\text{-Si}_3\text{N}_4$ ceramics was achieved through indirect AM. First, the lattice of Si-SiO_2 green body was printed via DIW, then the $\text{Si}_2\text{N}_2\text{O}\text{-Si}_3\text{N}_4$ ceramic was successfully prepared after the green body was sintered in nitrogen at a relatively low temperature. The formation mechanism of $\text{Si}_2\text{N}_2\text{O}$ and Si_3N_4 at 1250°C is shown in Figure 7E (reproduced with permission from Ref. [73] 2022 Elsevier). The as-obtained $\text{Si}_2\text{N}_2\text{O}\text{-Si}_3\text{N}_4$ ceramic had an apparent porosity of 42.73%, a compressive strength of 24.7 MPa, a dielectric constant of 4.89, and a loss tangent of .0054, respectively. Excellent dielectric properties were achieved due to the high porosity, the high proportion of $\text{Si}_2\text{N}_2\text{O}$ phase, and no residual silicon. Normally, almost all DIW research of Si_3N_4 ceramic was based on Si_3N_4 inks. However, DIW has high requirements for the rheology of ceramic ink. Clarkson et al.⁷⁴ created $\text{SiC/Si}_3\text{N}_4$ composites through UV-assisted DIW of a ceramic powder (Si_3N_4)-preceramic polymer (polycarbosilane) suspension, as shown in Figure 7F (reproduced with permission from Ref. [74] 2022 Elsevier). By coupling UV and DIW, the requirements for ink rheology were largely reduced to a certain extent. This article provided a reference for the preparation of complex-shaped ceramic composites by combining different AM techniques.

2.3.2 | Fused deposition modeling (FDM)

FDM process is a hot extrusion forming process, which involves heating wire composed of ceramic powder and polymer and extruding through a nozzle followed by solidification onto a forming table into the desired geometry. The basic process of FDM is shown in Figure 2F. FDM also has the advantages of material extrusion. However, the shortcoming of the low part surface accuracy is also obvious due to volume expansion during heating. In addition to this, the residue of FDM filament during heating can cause nozzle blockage.

Agarwala et al.⁷⁵ produced complex-shaped Si_3N_4 parts with high green density and high performance by FDM successfully, as shown in Figure 8A (reproduced with permission from Ref. [75] 1996 The University of Texas at Austin). It was shown that the binder in FDM-3D

printed green pieces could be removed and sintered to densities and strengths comparable to those achieved by traditional ceramic processing methods. This work had reference significance for FDM fabrication of Si_3N_4 ceramic components. However, build defects could be encountered in improperly built FDM-3D printed parts. Wu et al.⁷⁶ suggested that warm isostatic pressing (WIP'ing) at temperatures above 70°C might be effective in the elimination of build defects. However, after sintering, it was seen from the low fracture strength and the fracture surface features that the defects were still not completely healed. Although WIP'ing was successful in visibly removing internal voids in FDM-3D printed parts, their strength was still limited. Therefore, further investigations on the effects of pressure and temperature would be suggested. Rangarajan et al.⁷⁷ explored the rheological and mechanical properties required for a successful FDM feedstock material. At 185°C, the viscosity of filament feedstock with 55 vol.% was measured to be less than 50 Pa s in the shear rate range of 70–1128 s⁻¹. They also verified the ratio of the value of pressure to drive the extrusion to the filament buckling stress, $\Delta P/\sigma_E$, must be <1.1 for efficient pumping during FDM. It was necessary to quantitatively understand the relationship between ΔP and flow, geometric, and material rheological parameters for greater flow control during FDM. In their further paper,⁷⁸ dense, homogenous, near-net-shape Si_3N_4 parts were fabricated by using proper build parameters and printing routes. They identified and characterized build parameter-dependent heterogeneities and defects that arise from the FDM process and evaluated the effects of build orientation on the mechanical properties of structural Si_3N_4 parts made by FDM. The results showed that mechanical properties of Si_3N_4 parts were isotropic. Therefore, the mechanical properties of Si_3N_4 parts in specific directions could be enhanced by doping the FDM filament feedstock with $\beta\text{-Si}_3\text{N}_4$ seed particles. Similarly, McIntosh et al.⁷⁹ proved that warping of parts became a serious problem when using an all-aligned road vector build strategy (i.e., all 0° or all 90° road vectors). In contrast, using alternating +45°/-45° crosshatched road vectors could avoid warping. A schematic representation of warpage effects that resulting from is shown in Figure 8B (reproduced with permission from Ref. [79] 2008 John Wiley and Sons). Meanwhile, this article indicated the FDM process could be utilized to create advanced multifunctional ceramic components.

2.4 | Other additive manufacturing technologies

In addition to the aforementioned AM technologies, BJ and LOM were also reported to fabricate Si_3N_4 ceramic.

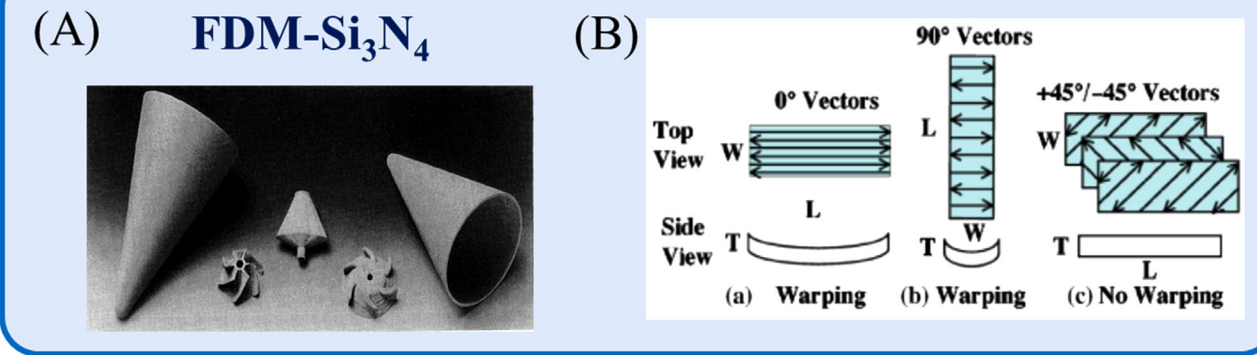


FIGURE 8 (A) Fused deposition modeling (FDM)-3D printed complex-shaped Si_3N_4 parts with high green density, (B) schematic representation of warpage effects. *Source:* (A) Reproduced with permission from Ref. [75] 1996 The University of Texas at Austin and (B) reproduced with permission from Ref. [79] 2008 John Wiley and Sons

2.4.1 | Binder jetting (BJ)

The procedure for the BJ of ceramic is presented in Figure 2G. During BJ, the roller spreads the ceramic powder of the powder tank under the nozzle. After that, the nozzle jets the binder to the predetermined areas. Then, the forming platform descends to a certain height, so back and forth. Finally, a 3D ceramic green body is formed on the forming platform. BJ has many potential advantages. For example, it can work with virtually any powdered feedstock and can incorporate FGMs.¹⁰¹ However, the density of parts made with BJ is usually very low. Therefore, most researchers use BJ to prepare porous Si_3N_4 ceramics.

Rabinskiy et al.⁸⁰ fabricated Si_3N_4 ceramics by indirect AM technology. First, they created silicon green body using BJ, and then porous Si_3N_4 ceramic was obtained using pressure less reaction sintering. However, the porosity of the as-sintered Si_3N_4 sample reached up to 70%, resulting in poor mechanical properties. In another paper,⁸¹ they investigated the effects of different types of binders on porosity and properties of samples. The results proved that denser and stronger specimens were prepared using a binder based on epoxy, compared to the water-based binder. The porosity of the porous Si_3N_4 sample prepared with epoxy-based binders was reduced to 30%–40%. They proposed to further reduce the porosity of green bodies and improved mechanical properties by additional compaction of green bodies.⁸² After additional compaction, the porosity of the porous Si_3N_4 ceramic decreased from 30%–40% to 15%–25%, and the flexural strength increased from 53 ± 2 to 77 ± 5 MPa, respectively. The results showed that the method of additional compaction was of great help in improving the mechanical properties of porous Si_3N_4 ceramic, which also confirmed that the mechanical properties of the as-sintered Si_3N_4 ceramic strongly depend on their porosity. To further study the relationship between

mechanical properties and porosity, Lurie et al.⁸³ analyzed the effects of porosity and pore shapes on the elastic properties of Si_3N_4 ceramic obtained by BJ and pressureless reaction sintering. Silicon green bodies in powder bed after BJ and Si_3N_4 ceramic samples after sintering is shown in Figure 9A (reproduced with permission from Ref. [83] 2017 Springer). They found that the low elastic modulus of the ceramics was mostly determined by the shape of the pores and their volume fraction. However, evaluation of the strength of the ceramic was a much more complicated problem, because it was difficult to establish a quantitative correlation between the changes in the elastic and strength properties of porous materials in the general case. Xiao et al.⁸⁴ synthesized a $(\text{SiC}_w\text{-}\text{Si}_3\text{N}_4_w)/(\text{Si}_3\text{N}_4\text{-SiC})$ composite via BJ, nitridation process, and a subsequent chemical vapor infiltration (CVI) process. They studied the effects of whiskers content on the mechanical properties. Compared to the bulks without whiskers, the result showed that the flexural strength increased by 63.6% when the SiC_w content was 3 wt.%. In addition to the poor mechanical properties of Si_3N_4 parts prepared by indirect BJ technology, this method also had many other limitations. Therefore, Cheng et al.⁸⁵ prepared Si_3N_4 ceramics by direct BJ and studied the effects of the deposition time and heat treatment of CVI on the microstructure and properties of porous $\text{Si}_3\text{N}_4\text{-Si}_3\text{N}_4$ composites. With increasing the deposition time, the weight and density of porous $\text{Si}_3\text{N}_4\text{-Si}_3\text{N}_4$ composite increased and the porosity decreased. In the future, it is hoped that more research should focus on direct BJ preparation of Si_3N_4 ceramic.

3DP not only has a similar jetting process to BJ but also has the same advantages and disadvantages (Figure 2H). Actually, 3DP is another name for BJ.

Li et al.⁸⁶ fabricated porous Si_3N_4 ceramic using techniques of oxidation-bonding combined with sol-gel infiltration sintering (OB-IS), cold-pressing combined with

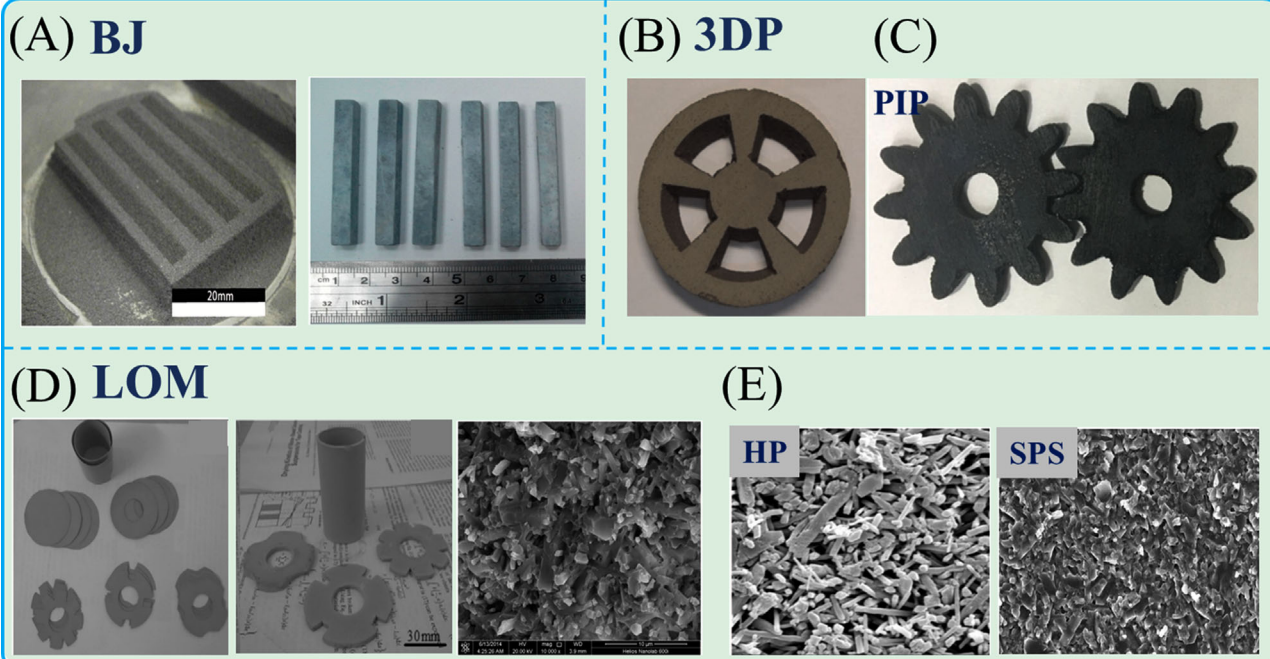


FIGURE 9 (A) Silicon green bodies in powder bed after binder jetting (BJ) and Si_3N_4 ceramic samples after sintering, (B) 3D printed Si_3N_4 part, (C) Si_3N_4 -SiOC ceramic with a complex shape by 3D printing (3DP) combined with direct nitridation and polymer infiltration and pyrolysis (PIP), (D) complicated shapes of green tapes and Si_3N_4 samples before and after sintering, (E) SEM images of Si_3N_4 samples sintered by hot pressing (HP) and spark plasma sintering (SPS). *Source:* (A) Reproduced with permission from Ref. [83] 2017 Springer; (B) reproduced with permission from Ref. [88] 2015 Elsevier; (C) reproduced with permission from Ref. [89] 2017 Springer; (D) reproduced with permission from Ref. [91] 2015 Elsevier; and (E) reproduced with permission from Ref. [93] 2006 Elsevier

pressureless sintering (CP-PS), and 3D-printing combined with pressureless sintering (3DP-PS). Comparing Si_3N_4 ceramics prepared by the other two techniques, the Si_3N_4 ceramic by 3DP-PS possessed a high porosity of 68% due to the incompact stack of Si_3N_4 particles in the preform. The porous Si_3N_4 ceramic by 3DP possessed excellent dielectric properties while showing poor mechanical properties (a flexural strength of 13 MPa, and a fracture toughness of .3 MPa $\text{m}^{1/2}$, respectively) due to the high porosity. Therefore, they used CVI to improve the mechanical properties of the porous Si_3N_4 ceramic in another study.⁸⁷ After CVI for 40 h, the mechanical properties of the porous Si_3N_4 ceramic were greatly improved (a flexural strength of 95 MPa, and a fracture toughness of 2.4 MPa $\text{cm}^{1/2}$, respectively) because of the increase in the connection strength among Si_3N_4 particles, whereas the dielectric properties were reduced slightly due to the slight decrease in porosity. The result showed that porous Si_3N_4 ceramic manufactured by 3DP combined with CVI was an excellent wave-transparent material. In addition to CVI, another possible way to enhance the mechanical properties of 3DP Si_3N_4 ceramic is to synthesize ceramic matrix composites. Duan et al.⁸⁸ fabricated twinned SiC nanowires reinforced Si_3N_4 composite by the combination of 3DP and polymer infiltration and pyrolysis (PIP). The as-prepared

Si_3N_4 part is shown in Figure 9B (reproduced with permission from Ref. [88] 2015 Elsevier). They investigated the effects of SiC nanowires on the microstructure, dielectric properties, and an absorption of the Si_3N_4 -SiC ceramic. The result showed that the lowest reflection coefficient of Si_3N_4 -SiC ceramic with 10.5-wt.% SiC attained 57 dB at the sample thickness of 2.3 mm, which indicating 99.999% of electromagnetic (EM) wave power was absorbed. This paper demonstrated that SiC nanowires-reinforced Si_3N_4 -SiC ceramic was a promising EM absorbing material. In their further article,⁸⁹ twinned SiC nanowires-reinforced Si_3N_4 -SiOC composites (as shown in Figure 9C [reproduced with permission from Ref. [89] 2017 Springer]) were successfully fabricated through a joint process of 3DP, direct nitridation, and PIP. The author not only designed complex-shaped Si_3N_4 -SiOC ceramic but also investigated its EM shielding and mechanical properties. With the increase of the infiltration cycle number, the porosity went down from 70% to 21%, the average SE_T (the total loss of the EM interference shielding) rose from 2 to 35 dB with a lower SE_R (the reflection loss) of 7 dB and higher SE_A (the absorption loss) of 28 dB. It was indicated that more than 99.9% of the EM energy was reflected and absorbed, and only less than .1% of the EM energy was transmitted. Meanwhile, the flexural strength reached 63 MPa. These

results demonstrated that the SiC nanowires-reinforced Si_3N_4 -SiOC ceramic was a promising EM shielding and structural material. This paper provided a reference for the structural-functional integration of additively manufactured Si_3N_4 ceramic.

2.4.2 | Laminated object manufacturing (LOM)

LOM forms parts by sheets as raw material. The basic process of LOM is shown in Figure 2I. In this process, individual sheets are rolled onto the forming platform, the binder is laid down on the sheet, and another sheet is then rolled onto the binder, fusing the two layers together. A laser then cuts the cross-sectional outline of the part only one layer in thickness into laminated sheets. The process is then repeated with successive layers. The excess material supports the part during the process and is removed during post-processing.¹⁰² This method offers considerable savings in cost and time. The key processing steps in the preparation of LOM Si_3N_4 components include Si_3N_4 tape fabrication, green shape forming using LOM, post-LOM processing, and densification.⁹⁰

Rodrigues et al.⁹⁰ demonstrated that LOM was a viable method for preparing functional Si_3N_4 ceramic with good physical and mechanical properties. The room temperature and high temperature (1260°C) flexural strengths of Si_3N_4 ceramic were in the range of 700–900 and 360–400 MPa, respectively, and the fracture toughness averaged from 5.5 to 7.5 $\text{MPa m}^{1/2}$, which were comparable to those reported for conventionally prepared Si_3N_4 ceramics. Domestic Liu et al.⁹¹ also proved the feasibility of preparing Si_3N_4 ceramic components by aqueous tape casting in combination with LOM. Complicated shapes of green tapes and Si_3N_4 samples before and after sintering and section view of the Si_3N_4 components are shown in Figure 9D (reproduced with permission from Ref. [91] 2015 Elsevier). A relatively high density (~93.7%) and good strength (~475 MPa) of the sintered components were obtained. Park et al.⁹² fabricated a complex-shaped Si_3N_4 part with aligned whisker seeds using LOM. CIP was used to make dense ceramic components. The results showed that the body was sintered to 98.5% of theoretical density, and the Vickers hardness was $13.9 \pm .3$ GPa. The fracture toughness values parallel and perpendicular to the stacking direction were $6.1 \pm .4$ and $5.2 \pm .2$ $\text{MPa m}^{1/2}$, respectively. Zhang et al.⁹³ prepared Si_3N_4 samples through aqueous tape casting, laminating, hot pressing (HP), and spark plasma sintering (SPS). SEM images of the Si_3N_4 samples by HP and SPS are shown in Figure 9E (reproduced with permission from Ref. [93] 2006 Elsevier). Both HP and SPS were proved to be effective for densifying

Si_3N_4 samples. Si_3N_4 samples sintered by SPS exhibited a higher fracture toughness ($8.1 \pm .3$ $\text{MPa m}^{1/2}$), whereas a lower strength (650 ± 23 MPa) than that sintered by HP ($7.6 \pm .4$ $\text{MPa m}^{1/2}$, 725 ± 26 MPa). In addition to improving performance by increasing density, Pope et al.⁹⁴ designed three microstructural variants (second-phase interface compositions, FGMs, and oriented microstructures) to enhance the properties of the multilayer Si_3N_4 structure. The results confirmed that all three methods could play a role in improving mechanical properties. Among the three structural design methods (second-phase interface compositions, FGMs, and oriented microstructures), interface design is the most common method, because the introduction of interfacial second-phase materials improved performance while considering the designability.

3 | PERSPECTIVES

Based on the previous summary of the current advances of AM technologies of Si_3N_4 ceramic, prospects are forecasted.

3.1 | Densification and strengthening

As we all know, Si_3N_4 ceramic is difficult to densify because of the covalent nature of Si–N bonding. Moreover, some AM techniques are prone to a lot of defects during the manufacturing process, which will also affect the density and mechanical performance of the ceramic products.

During AM, it is important to quantitatively characterize and analyze the defects within ceramic. X-ray-computed tomography (X-CT) can provide adequate information on the defect distribution of the material. Lüchtenborg et al.⁵¹ generated Si_3N_4 ceramic green bodies with high particle packing density using LIS casting. Meanwhile, a whole sample and a bending bar were characterized using μ CT to determine density and local pore distribution, as shown in Figure 10A (reproduced with permission from Ref. [51] 2017 Goeller). In the μ CT scan of an entire sample, pores with a hemispherical shape and larger flat areas of flaws were visible. The diameter of these pores reached $420 \mu\text{m}$ and delaminations or cracks located parallel to each other and parallel to the layers. The porosity of the part was calculated to be $.41\% \pm .47\%$. In the μ CT scan of a bending bar sample, large and small pores were detected, and the largest pore has a diameter of $420 \mu\text{m}$. A large part of the reason for the low number of defects in LIS is that there was no photosensitive resin in the paste required for LIS. Diener et al.¹⁰³ investigated the influence of DIW printing patterns on residual pore sizes and pore distributions by X-ray microtomography and tried to establish the

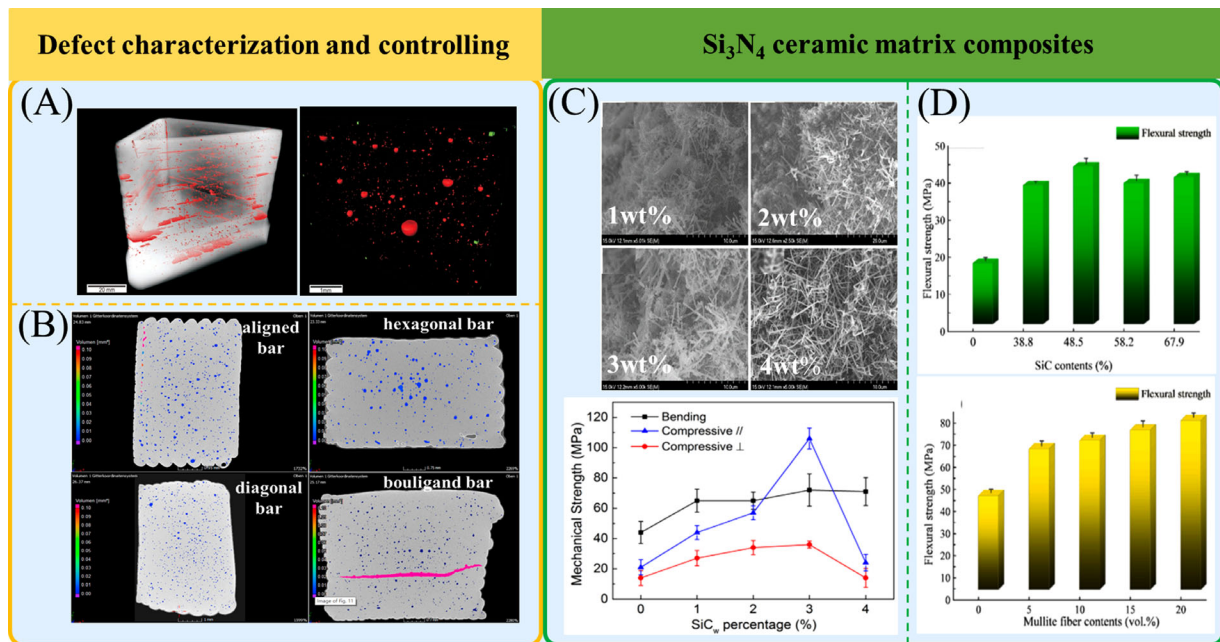


FIGURE 10 (A) μ CT reconstruction of a scan of a whole Si_3N_4 sample and a part of a bending bar, (B) μ CT image of a cross section taken at the middle of sintered bars manufactured using different printing patterns, (C) the microstructures of fabricated $(\text{SiC}_w\text{-}\text{Si}_3\text{N}_4w)/(\text{Si}_3\text{N}_4\text{-}\text{SiC})$ composite and the bending strength, out-plane (\perp) and in-plane ($/\!/$) compressive strengths of the composites with different SiC_w contents, (D) the effects of the SiC mass fraction and the addition of Al_2O_3 and mullite fibers on the properties of the $\text{Si}_3\text{N}_4\text{-}\text{SiC}/\text{SiO}_2$ composites. *Source:* (A) Reproduced with permission from Ref. [51] 2017 Goeller; (B) reproduced with permission from Ref. [103] 2021 Elsevier; (C) reproduced with permission from Ref. [84] 2018 Elsevier; and (D) reproduced with permission from Ref. [47] 2021 Elsevier

relationship between the residual pore structure and the printing parameters. μ CT image of a cross section taken at the middle of sintered bars manufactured using different printing patterns is shown in Figure 10B (reproduced with permission from Ref. [103] 2021 Elsevier). No clear effect on the final pore characteristics of Si_3N_4 bars fabricated using different printing patterns was observed. However, adjusting the distance between adjacent filament centers and changing the ink rheology can help reduce the final porosity of sintered Si_3N_4 parts. In summary, we can achieve the purpose of densification and strengthening through defect characterization and controlling.

During sintering process, the density of the as-obtained Si_3N_4 ceramic is generally difficult to be completely dense by pressureless sintering. Generally, pressure sintering, reaction sintering, CVI, SPS, and HP are used to promote the densification of Si_3N_4 ceramic. Table 1 lists and compares the relative density, strength, and fracture toughness of Si_3N_4 ceramics prepared by different AM technologies.

The reason for the higher density and strength of Si_3N_4 prepared by LIS and LOM was high curing thickness and applied pressure, respectively. Another approach to strengthening and toughening was to prepare Si_3N_4 -based ceramic composites by adding a second phase into the Si_3N_4 ceramic matrix. Duan et al.⁸⁸ fabricated porous Si_3N_4 composites reinforced with in situ-formed

twinning SiC nanowires by 3DP and PIP to improve both the real and the imaginary parts of permittivity. They demonstrated that $\text{SiC}_{\text{NWS}}\text{-}\text{Si}_3\text{N}_4$ ceramics had a superior microwave-absorbing ability. Xiao et al.⁸⁴ investigated the effect of SiC_w content on the mechanical performance of porous $(\text{SiC}_w\text{-}\text{Si}_3\text{N}_4w)/(\text{Si}_3\text{N}_4\text{-}\text{SiC})$ composite by BJ and CVI. The microstructures of the as-fabricated $(\text{SiC}_w\text{-}\text{Si}_3\text{N}_4w)/(\text{Si}_3\text{N}_4\text{-}\text{SiC})$ composite and the flexural strength, out-plane (\perp) and in-plane ($/\!/$) compressive strengths of the composites with different SiC_w contents are shown in Figure 10C (reproduced with permission from Ref. [84] 2018 Elsevier). The flexural strength increased monotonously in the interval from 0 to 3 wt.%, which indicated that SiC_w presented a good strengthening effect in this range. In addition to fiber-reinforced ceramic matrix composites, Yu et al.⁴⁷ successfully manufactured $\text{Si}_3\text{N}_4\text{-}\text{SiC}/\text{SiO}_2$ composite part by SLS and infiltration processes and investigated the effects of the SiC mass fraction and the addition of mullite fibers on the properties of the $\text{Si}_3\text{N}_4\text{-}\text{SiC}/\text{SiO}_2$ composites. Figure 10D (reproduced with permission from Ref. [47] 2021 Elsevier) showed that with an increase in the mass fraction of SiC , the flexural strength of the samples increased to the maximum value of 42.45 MPa at 48.5-wt.% SiC first and then decreased. The flexural strength of the $\text{Si}_3\text{N}_4\text{-}\text{SiC}/\text{SiO}_2$ composites improved significantly with

TABLE 1 Comparison of the relative density, strength, and fracture toughness of Si_3N_4 ceramics fabricated by different additive manufacturing (AM) techniques

Material	AM technology	Posttreatment	Relative density (%)	Strength (MPa)	Fracture toughness (MPa m ^{1/2})	Ref.
$\text{Si}_3\text{N}_4\text{--SiC/SiO}_2$	SLS	Sol-infiltration	92.05	42.4 ^a	–	47
Si_3N_4	LIS	Pressure sintering	99.4	323 ^b	–	51
Si_3N_4	DLP	Pyrolysis	88.43	57.3 ± 8.7 ^a	–	52
Si_3N_4	DLP	Pressure sintering	95	–	5.82 ± .42	56
Si_3N_4	DLP	Pressureless sintering	85.4 ± .3	149.2 ± 1.9 ^a	–	59
Si_3N_4	DLP	Field-assisted sintering	95.8	–	6.57 ± .07	63
$\text{Si}_3\text{N}_4\text{--SiO}_2$	DLP	Pressureless sintering	82.3	77 ± 5 ^a	–	65
$\text{Si}_2\text{N}_2\text{O--Si}_3\text{N}_4$	DIW	Reaction sintering	57.27	16.9 ^a 24.7 ^c	–	73
Porous Si_3N_4	BJ	Pressureless sintering	60 – 70	53 ± 2 ^a	–	82
Porous Si_3N_4	3DP	CVI	63.98	47 ± 2 ^a	–	86
Porous Si_3N_4	3DP	Pressureless sintering + CVI	39	95 ^a	2.4	87
Si_3N_4	LOM	Pressure sintering	93.7	475 ^a	–	91
Si_3N_4	LOM	HP	99.72	725 ± 26 ^a	7.6 ± .4	93
		SPS	99.78	650 ± 23 ^a	8.1 ± .3	

Abbreviations: 3DP, 3D printing; BJ, binder jetting; CVI, chemical vapor infiltration; DIW, direct ink writing; HP, hot pressing; LIS, laser-induced slip; LOM, laminated object manufacturing; SLS, selective laser sintering; SPS, spark plasma sintering.

^aThree-point flexural strength.

^bFour-point flexural strength.

^cCompressive strength.

the addition of mullite fibers, and the incorporation of the mullite fibers played an important role in improving the mechanical properties of the $\text{Si}_3\text{N}_4\text{--SiC/SiO}_2$ composites. Usually, there are mainly two types of AM technologies for fiber-reinforced Si_3N_4 ceramic matrix composites: indirect AM and direct AM. The indirect AM methods first prepare the Si_3N_4 ceramic green body by common AM technologies, then fabricate the composite green part via in situ reactions, and finally sinter to obtain the final body. Different from indirect AM, direct AM methods including fabrication of fiber reinforced Si_3N_4 ceramic matrix composite green part by various AM technologies, debinding, and sintering. Whether indirect AM or direct AM, the introduction of high-strength, high elasticity fibers (including short and continuous fibers) as reinforcements is an effective method to improve the toughness and reliability of Si_3N_4 ceramics.¹⁰⁴ In the future, AM of fiber-reinforced Si_3N_4 ceramics will have broad prospects due to its excellent material properties and wide application.

3.2 | Functional design

Si_3N_4 ceramic has excellent EM properties and biological properties. Most researchers only focus on its

mechanical properties; however, there are only a few studies on the EM properties and biological properties of additively manufactured Si_3N_4 .

Chen et al.⁶⁵ studied the effect of sintering temperature on the real permittivity and the tangent loss of $\text{Si}_3\text{N}_4\text{--SiO}_2$ (as shown in Figure 11A (reproduced with permission from Ref. [65] 2021 Elsevier)). The real permittivity reached a maximum value at 1350°C and the minimum value at 1250°C, and the tangent loss decreased with the increase of temperature. Lower $\tan \delta$ means better transmission rate, which indicated that $\text{Si}_3\text{N}_4\text{--SiO}_2$ could be a potential transparent material. Cheng et al.⁸⁵ indicated the excellent EM wave-transparent performance of porous $\text{Si}_3\text{N}_4\text{--Si}_3\text{N}_4$ composite ceramics (as shown in Figure 11B (reproduced with permission from Ref. [85] 2015 Elsevier)). When the CVI processing time was increased from 0 to 12 h, the dielectric constant gradually increased from 1.72 to 3.60; however, the dielectric loss always remained less than .01. After heat treatment, the dielectric constant got a slight increase from 3.60 to 3.70 with the dielectric loss still maintaining lower than .01. Duan et al.⁸⁹ also investigated EM interference shielding properties of $\text{Si}_3\text{N}_4\text{--SiOC}$ composites. A schematic illustration of the shielding mechanism in $\text{Si}_3\text{N}_4\text{--SiOC}$ ceramics is shown in Figure 11C (reproduced with permission from Ref. [89] 2017 Springer). Zanocco et al.⁴⁹ also produced an antibacterial and

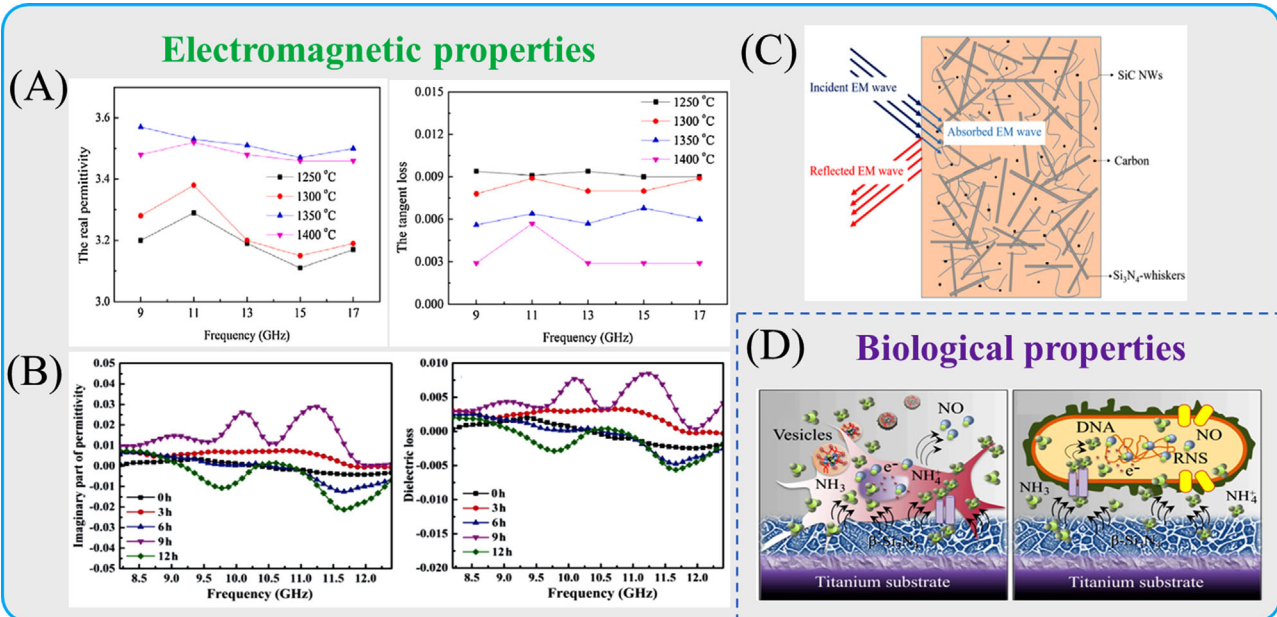


FIGURE 11 (A) Dielectric constant of Si_3N_4 – SiO_2 ceramics, (B) dielectric properties in 8.2–12.4 GHz of porous Si_3N_4 – Si_3N_4 composite ceramics, (C) schematic illustration of the shielding mechanism in Si_3N_4 –SiOC ceramics, (D) schematic draft of osteoblast and bacteria interactions at the biomolecular interface with Si_3N_4 . Source: (A) Reproduced with permission from Ref. [65] 2021 Elsevier; (B) reproduced with permission from Ref. [85] 2015 Elsevier; (C) reproduced with permission from Ref. [89] 2017 Springer; and (D) reproduced with permission from Ref. [49] 2020 Elsevier

osteogenic Si_3N_4 coating on an orthopedic titanium substrate. The Si_3N_4 coating showed concurrent osteogenic and antibacterial behaviors similar to those observed in bulk Si_3N_4 bioceramic implants. A schematic draft of osteoblast and bacteria interactions at the biomolecular interface with Si_3N_4 is shown in Figure 11D (reproduced with permission from Ref. [49] 2020 Elsevier). Zhao et al.⁷⁰ fabricated Si_3N_4 implants with a fibrous surface morphology or surface roughness by DIW, which had been found to have a beneficial effect in endowing Si_3N_4 implants with antibacterial activity. Sainz et al.⁷¹ manufactured 3D- Si_3N_4 scaffolds intended for bone tissue engineering by DIW. They demonstrated the feasibility of 3D- Si_3N_4 printed materials as robust scaffolds with a high bioactivity and affinity for proteins and confirmed its potential application for bone tissue engineering. Compared to mechanical properties, EM and biological properties require Si_3N_4 components to have a certain porosity. At present, most researchers usually use material extrusion technology to additively manufacture porous Si_3N_4 . These techniques not only have the disadvantage of low precision but also result in lower mechanical properties of the final sample. Therefore, realizing the functional design of mechanical properties, EM and biological properties at the same time through other AM techniques or adding pore-forming agents will be the focus of many researchers in the future.

3.3 | Structure–function integration

In addition to realizing the functional design of materials, the biggest feature of AM is that it can achieve flexible design of structures, which has also attracted the attention of a large number of researchers.

DLP-based additively manufactured Al_2O_3 ceramic lattice structures (CLSs) with different structural configurations were in the work of Zhang et al.¹⁰⁵ They designed and fabricated three structural configurations of body-centered cubic, octet, and modified body-centered cubic, as shown in Figure 12A (reproduced with permission from Ref. [105] 2022 Taylor and Francis Ltd.). Moreover, the effect of structural configuration on the mechanical properties and failure modes of CLS was systematically studied in their work. Minasyan et al.⁴⁴ also additively manufactured mesostructured MoSi_2 – Si_3N_4 ceramic lattice through an SLM approach (as shown in Figure 12B (reproduced with permission from Ref. [44] 2019 Elsevier)). However, they only cared about the parameters of the SLM process, particularly the laser current, which have a significant effect on the internal and external architecture of the lattices. The effect of structure on performance needs to be further explored. In a word, AM can not only realize complex-shaped ceramic components but also realize the structural and functional design of ceramic. For detailed reports on additively manufactured ceramic

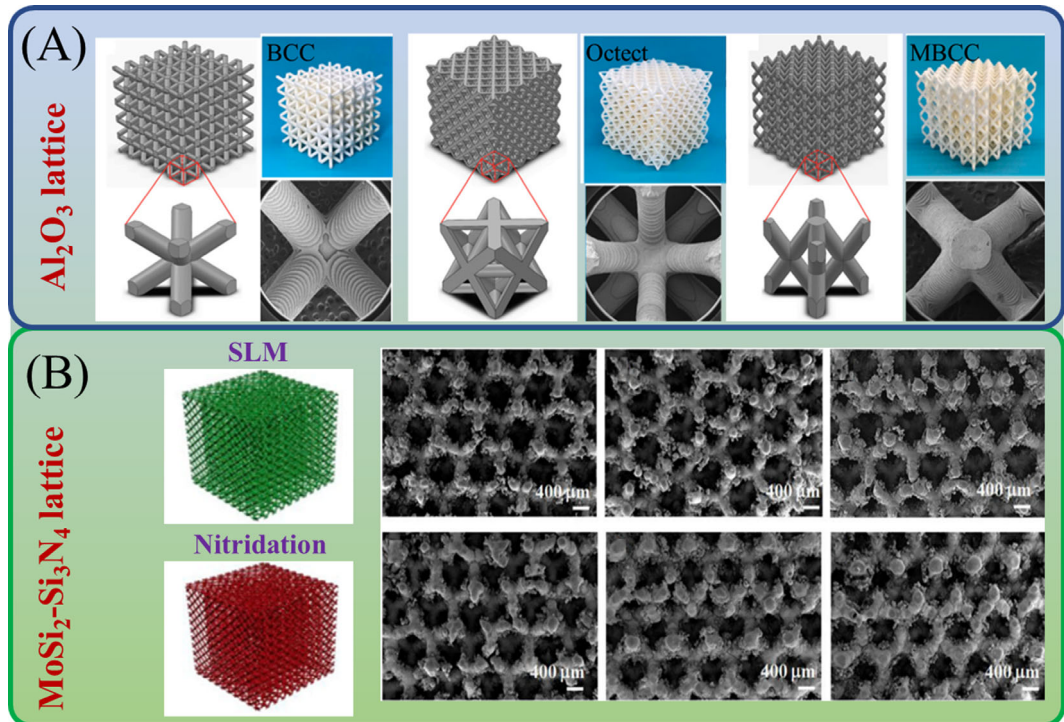


FIGURE 12 (A) Three Al_2O_3 ceramic structural configurations of body-centered cubic (BCC), octet, and modified body-centered cubic (MBCC), (B) mesostructured $\text{MoSi}_2-\text{Si}_3\text{N}_4$ ceramic lattice and SEM images of MoSi_2 -13-wt.% Si lattices sintered at different laser currents.
Source: (A) Reproduced with permission from Ref. [105] 2022 Taylor and Francis Ltd. and (B) reproduced with permission from Ref. [44] 2019 Elsevier

structures and structure–function integration, please refer to another review.¹⁰⁶ With the deepening of research, it will be a hot topic for future research that achieves external functional regulation by tailoring advanced structures (namely: structure–function integration).

4 | SUMMARY

Si_3N_4 ceramic has been widely applied in military, mechanical engineering, aerospace, and biomedical fields owing to their promising combined properties of excellent mechanical properties and thermal shock resistance at elevated temperatures, and good dielectric properties and biocompatibility. Traditional Si_3N_4 preparation methods have certain limitations in the preparation of complex structures. The emergence of AM technology provides an innovative technological approach for the fabrication of complex special-shaped Si_3N_4 ceramic materials and structures. In this paper, the research progress of Si_3N_4 ceramic AM is systematically and comprehensively summarized. The key scientific and technological challenges and the future research opportunities for the AM of Si_3N_4 ceramic are analyzed. To sum up, this review is aimed to give some guidance for the study of the AM of Si_3N_4 ceramic.

ACKNOWLEDGMENTS

Financial supports from the National Natural Science Foundation of China (Grant nos. 51772028, 91960102), and the Open Project of State Key Laboratory of Explosion Science and Technology (Grant no. QNKT22-15) was also sincerely appreciated.

ORCID

Ruijie He <https://orcid.org/0000-0003-2498-2363>

REFERENCES

- Zhang RB, Fang DN, Chen XM, Pei YM. Effect of pre-oxidation on the microstructure, mechanical and dielectric properties of highly porous silicon nitride ceramics. *Ceram Int*. 2012;38:6021–6. <https://doi.org/10.1016/j.ceramint.2012.03.056>
- Collins JF, Gerby RW. New refractory uses for silicon nitride reported. *JOM*. 1955;7:612–15. <https://doi.org/10.1007/BF03377548>
- Vikulin VV. Production of Si_3N_4 -based articles and their application in aerospace industry. *Adv Sci Technol*. 2006;45:1751–8. <https://doi.org/10.4028/www.scientific.net/AST.45.1751>
- Bocanegra-Bernal MH, Matovic B. Dense and near-net-shape fabrication of Si_3N_4 ceramics. *Mater Sci Eng A—Struct*. 2009;500:130–49. <https://doi.org/10.1016/j.msea.2008.09.015>
- Heimann RB. Silicon nitride, a close to ideal ceramic material for medical application. *Ceramics*. 2021;4:208–23. <https://doi.org/10.3390/ceramics4020016>

6. Xue WJ, Yi J, Xie ZP, Liu W, Chen J. Enhanced fracture toughness of silicon nitride ceramics at cryogenic temperatures. *Scr Mater.* 2012;66:891–4. <https://doi.org/10.1016/j.scriptamat.2012.02.007>
7. Tan DW, Zhu LL, Wei WX, Yu JJ, Zhou YZ, Guo WM, et al. Performance improvement of Si_3N_4 ceramic cutting tools by tailoring of phase composition and microstructure. *Ceram Int.* 2020;46:26182–9. <https://doi.org/10.1016/j.ceramint.2020.07.116>
8. da Silva CRM, Pereira Reis DA, dos Santos C. Creep of heat treated silicon nitride with neodymium and yttrium oxides additions. *Mat Sci Eng A—Struct.* 2010;527:6893–8. <https://doi.org/10.1016/j.msea.2010.07.044>
9. Tian XH, Yan KC, Zhao J, Cheng YH, Wang ZB. Thermal and mechanical shock resistances of $\text{Si}_3\text{N}_4/(W, \text{Ti})\text{C}$ graded nanocomposite ceramic tool material. *Ceram Int.* 2020;46:2317–24. <https://doi.org/10.1016/j.ceramint.2019.09.222>
10. Tyuganova MA, Zubkova NS, Butylkina NG. Polymeric fibre materials with low combustibility – a review. *Fibre Chem.* 1994;26:294–305. <https://doi.org/10.1007/BF02396597>
11. Riley FL. Silicon nitride and related materials. *J Am Ceram Soc.* 2000;83(2):245–65. <https://doi.org/10.1111/j.1151-2916.2000.tb01182.x>
12. Hampshire S. Silicon nitride ceramics-review of structure, processing and properties. *J Achieve Mater Manuf Eng.* 2007;24(1):43–50. jamme.acmssse.h2.pl/papers_vol24_1/24104.pdf
13. Terwilliger GR, Lange FF. Pressureless sintering of Si_3N_4 . *J Mater Sci.* 1975;10:1169–74. <https://doi.org/10.1007/BF00541399>
14. Luo CX, Zhang YX, Deng TF. Pressureless sintering of high-performance silicon nitride ceramics at 1620°C. *Ceram Int.* 2021;47:29371–8. <https://doi.org/10.1016/j.ceramint.2021.07.104>
15. Xue JM, Liu Q, Gui LH. Lower-temperature hot-pressed dy- α -sialon ceramics with an LiF additive. *J Am Ceram Soc.* 2007;90(5):1623–5. <https://doi.org/10.1111/j.1151-2916.2007.01558.x>
16. Lin RL, Bao WC, Yu JJ, Guo WM, Lin HT. Effect of ZrB_2 and its oxide impurities (ZrO_2 and B_2O_3) on hot-pressed Si_3N_4 ceramics at low temperature. *J Eur Ceram Soc.* 2021;41:6763–6. <https://doi.org/10.1016/j.jeurceramsoc.2021.06.041>
17. Hoffmann MJ. Relationship between microstructure and mechanical properties of silicon nitride ceramics. *Pure Appl Chem.* 1995;67(6):939–46. <https://doi.org/10.1351/pac199567060939>
18. Liao SJ, Zhuang YH, Wang JJ, Jiang CX, Zhou LJ, Li S, et al. Synergistic effect of binary fluoride sintering additives on the properties of silicon nitride ceramics. *Ceram Int.* 2022;48(15):21873–86. <https://doi.org/10.1016/j.ceramint.2022.04.167>
19. Wang LJ, Qiao ZH, Qi Q, Yu Y, Li TY, Liu XJ, et al. Improving abrasive wear resistance of Si_3N_4 ceramics with self-matching through tungsten induced tribochemical wear. *Wear.* 2022;494–495:204254. <https://doi.org/10.1016/j.wear.2022.204254>
20. Aguirre TG, Cramer CL, Mitchell DJ. Review of additive manufacturing and densification techniques for the net- and near net-shaping of geometrically complex silicon nitride components. *J Eur Ceram Soc.* 2022;42:735–43. <https://doi.org/10.1016/j.jeurceramsoc.2021.11.001>
21. Neil JT, French KW, Quackenbush CL, Smith JT. Fabrication of turbine components and properties of sintered silicon nitride. *ASME.* 1982;5:18–22. <https://doi.org/10.1115/82-GT-252>
22. Bandyopadhyay G, French KW. Fabrication of near-net-shape silicon nitride parts for engine application. *J Eng Gas Turbines Power.* 1986;108(3):536–9. <https://doi.org/10.1115/1.3239943>
23. Janney MA, Omatete OO, Walls CA, Nunn SD, Ogle RJ, Westmoreland G. Development of low-toxicity gelcasting systems. *J Am Ceram Soc.* 1998;81(3):581–91. <https://doi.org/10.1111/j.1151-2916.1998.tb02377.x>
24. Wan T, Yao DX, Hu HL, Xia YF, Zuo KH, Zeng YP. Fabrication of porous Si_3N_4 ceramics through a novel gelcasting method. *Mater Lett.* 2014;133:190–2. <https://doi.org/10.1016/j.matlet.2014.06.182>
25. Prakash KS, Nancharaih T, Rao VVS. Additive manufacturing techniques in manufacturing—an overview. *Mater Today: Proc.* 2018;5:3873–82. <https://doi.org/10.1016/j.matpr.2017.11.642>
26. Zhang KQ, He RJ, Ding GJ, Bai XJ, Fang DN. Effects of fine grains and sintering additives on stereolithography additive manufactured Al_2O_3 ceramic. *Ceram Int.* 2021;47:2303–10. <https://doi.org/10.1016/j.ceramint.2020.09.071>
27. Nie GL, Li YH, Sheng PF, Zuo F, Wu HL, Liu LR, et al. Microstructure refinement-homogenization and flexural strength improvement of Al_2O_3 ceramics fabricated by DLP-stereolithography integrated with chemical precipitation coating process. *J Adv Ceram.* 2021;10:790–808. <https://doi.org/10.1007/s40145-021-0473-2>
28. Zhang KQ, He RJ, Xie C, Wang G, Ding GJ, Wang M, et al. Photosensitive ZrO_2 suspensions for stereolithography. *Ceram Int.* 2019;45:12189–95. <https://doi.org/10.1016/j.ceramint.2019.03.123>
29. Zhang KQ, Meng QY, Zhang XQ, Qu ZL, Jing SK, He RJ. Roles of solid loading in stereolithography additive manufacturing of ZrO_2 ceramic. *Int J Refract Met Hard Mater.* 2021;99:105604. <https://doi.org/10.1016/j.ijrmhm.2021.105604>
30. Xing HY, Zou B, Li SS, Fu XS. Study on surface quality, precision and mechanical properties of 3D printed ZrO_2 ceramic components by laser scanning stereolithography. *Ceram Int.* 2017;43:16340–7. <https://doi.org/10.1016/j.ceramint.2017.09.007>
31. Huang K, Elsayed H, Franchin G, Colombo P. 3D printing of polymer-derived SiOC with hierarchical and tunable porosity. *Addit Manuf.* 2020;36:101549. <https://doi.org/10.1016/j.addma.2020.101549>
32. He C, Ma C, Li XL, Yan LW, Hou F, Liu JC, et al. Polymer-derived SiOC ceramic lattice with thick struts prepared by digital light processing. *Addit Manuf.* 2020;35:101366. <https://doi.org/10.1016/j.addma.2020.101366>
33. Jana P, Santoliquido O, Ortona A, Colombo P, Soraru GD. Polymer-derived SiCN cellular structures from replica of 3D printed lattices. *J Am Ceram Soc.* 2018;101(7):2732–8. <https://doi.org/10.1111/jace.15533>
34. Gyak KW, Vishwakarma NK, Hwang YH, Kim J, Yun HS, Kim DP. 3D-printed monolithic SiCN ceramic microreactors from a photocurable preceramic resin for the high temperature ammonia cracking process. *React Chem Eng.* 2019;4:1393–9. <https://doi.org/10.1039/C9RE00201D>
35. Feng CW, Zhang KQ, He RJ, Ding GJ, Xia M, Jin XX, et al. Additive manufacturing of hydroxyapatite bioceramic scaffolds: dispersion, digital light processing, sintering, mechanical properties, and biocompatibility. *J Adv Ceram.* 2020;9(3):360–73. <https://doi.org/10.1007/s40145-020-0375-8>
36. Yao YX, Qin W, Xing BH, Sha N, Jiao T, Zhao Z. High performance hydroxyapatite ceramics and a triply periodic minimum

- surface structure fabricated by digital light processing 3D printing. *J Adv Ceram.* 2021;10:39–48. <https://doi.org/10.1007/s40145-020-0415-4>
37. Cox SC, Jamshidi P, Eisenstein NM, Webber MA, Hassanin H, Attallah MM, et al. Adding functionality with additive manufacturing: fabrication of titanium-based antibiotic eluting implants. *Mat Sci Eng C—Mater.* 2016;64:407–15. <https://doi.org/10.1016/j.msec.2016.04.006>
38. Wei YH, Zhao DY, Cao QL, Wang J, Wu YH, Yuan B, et al. Stereolithography-based additive manufacturing of high-performance osteoinductive calcium phosphate ceramics by a digital light-processing system. *ACS Biomater Sci Eng.* 2020;6:1787–97. <https://doi.org/10.1021/acsbiomaterials.9b01663>
39. Mei H, Zhao X, Zhou SX, Han DY, Xiao SS, Cheng LF. 3D-printed oblique honeycomb $\text{Al}_2\text{O}_3/\text{SiC}_w$ structure for electromagnetic wave absorption. *Chem Eng J.* 2019;372:940–5. <https://doi.org/10.1016/j.cej.2019.05.011>
40. Xing HY, Zou B, Wang XF, Hu YF, Huang CZ, Xue K. Fabrication and characterization of SiC whiskers toughened Al_2O_3 paste for stereolithography 3D printing applications. *J Alloys Compd.* 2020;828:154347. <https://doi.org/10.1016/j.jallcom.2020.154347>
41. Wang WQ, Bai XJ, Zhang L, Jing SK, Shen CJ, He RJ. Additive manufacturing of C_{sf}/SiC composites with high fiber content by direct ink writing and liquid silicon infiltration. *Ceram Int.* 2022;48:3895–903. <https://doi.org/10.1016/j.ceramint.2021.10.176>
42. Al-Aj rash SMN, Browning C, Eckerle R, Cao L. Innovative procedure for 3D printing of hybrid silicon carbide/carbon fiber nanocomposites. *Nano Select.* 2021;2(11):2201–8. <https://doi.org/10.1002/nano.202100011>
43. Minasyan T, Liu L, Aghayan M, Kollo L, Kamboj N, Aydinyan S, et al. A novel approach to fabricate Si_3N_4 by selective laser melting. *Ceram Int.* 2018;44:13689–94. <https://doi.org/10.1016/j.ceramint.2018.04.208>
44. Minasyan T, Liu L, Holovenko Y, Aydinyan S, Hussainova I. Additively manufactured mesostructured $\text{MoSi}_2\text{-Si}_3\text{N}_4$ ceramic lattice. *Ceram Int.* 2019;45:9926–33. <https://doi.org/10.1016/j.ceramint.2019.02.035>
45. Wei ZH, Cheng LJ, Ma YX, Chen AN, Guo XF, Wu JM, et al. Direct fabrication mechanism of pre-sintered Si_3N_4 ceramic with ultra-high porosity by laser additive manufacturing. *Scr Mater.* 2019;173:91–5. <https://doi.org/10.1016/j.scriptamat.2019.07.046>
46. Wang KJ, Bao CG, Zhang CY, Li YH, Liu RZ, Xu HM, et al. Preparation of high-strength Si_3N_4 antenna window using selective laser sintering. *Ceram Int.* 2021;47:31277–85. <https://doi.org/10.1016/j.ceramint.2021.07.304>
47. Yu SW, Zeng T, Pan XT, Wu RN, Fan ML, Xu GD, et al. Fabrication of $\text{Si}_3\text{N}_4\text{-SiC/SiO}_2$ composites using 3D printing and infiltration processing. *Ceram Int.* 2021;47:28218–25. <https://doi.org/10.1016/j.ceramint.2021.06.235>
48. Qi H, He CG, Zhang PZ, Han WY, Guo FQ, Wu F, et al. Additive manufacturing of silicon nitride ceramic floatation spheres with excellent mechanical properties. *Materials.* 2019;12(17):2717. <https://doi.org/10.3390/ma12172717>
49. Zanocco M, Boschetto F, Zhu WL, Marin E, McEntire BJ, Bal BS, et al. 3D-additive deposition of an antibacterial and osteogenic silicon nitride coating on orthopaedic titanium substrate. *J Mech Behav Biomed.* 2020;103:103557. <https://doi.org/10.1016/j.jmbbm.2019.103557>
50. Xing HY, Zou B, Liu XY, Wang XF, Huang CZ, Hu YF. Fabrication strategy of complicated $\text{Al}_2\text{O}_3\text{-Si}_3\text{N}_4$ functionally graded materials by stereolithography 3D printing. *J Eur Ceram Soc.* 2020;40:5797–809. <https://doi.org/10.1016/j.jeurceramsoc.2020.05.022>
51. Lüchtenborg J, Mühlner T, Leonard F, Günster J. Laser-induced slip casting (LIS) – a new additive manufacturing process for dense ceramics demonstrated with Si_3N_4 . *J Ceram Sci Technol.* 2017;08(4):531–40. <https://doi.org/10.1016/j.jeurceramsoc.2020.05.022>
52. Wang M, Xie C, He RJ, Ding GJ, Zhang KQ, Wang G, et al. Polymer-derived silicon nitride ceramics by digital light processing based additive manufacturing. *J Am Ceram Soc.* 2019;102(9):5117–26. <https://doi.org/10.1111/jace.16389>
53. Li XB, Zhang JX, Duan YS, Liu N, Jiang JH, Ma RX, et al. Rheology and curability characterization of photosensitive slurries for 3D Printing of Si_3N_4 Ceramics. *Appl Sci.* 2020;10:6438. <https://doi.org/10.3390/app10186438>
54. Li YH, Huang SW, Wang SL, Zhang XY, Wang YL, Lu BW, et al. Research on the effects of surface modification of ceramic powder on cure performance during digital light processing (DLP). *Ceram Int.* 2022;48:3652–8. <https://doi.org/10.1016/j.ceramint.2021.10.146>
55. Huang RJ, Jiang QG, Wu HD, Li YH, Liu WY, Lu XX. Fabrication of complex shaped ceramic parts with surface-oxidized Si_3N_4 powder via digital light processing based stereolithography method. *Ceram Int.* 2019;45:5158–62. <https://doi.org/10.1016/j.ceramint.2018.11.116>
56. Liu Y, Zhan LN, He Y, Zhang J, Hu JJ, Cheng LJ, et al. Stereolithographical fabrication of dense Si_3N_4 ceramics by slurry optimization and pressure sintering. *Ceram Int.* 2020;46:2063–71. <https://doi.org/10.1016/j.ceramint.2019.09.186>
57. Liu Y, Cheng LJ, Li H, Li Q, Shi Y, Liu F, et al. Formation mechanism of stereolithography of Si_3N_4 slurry using silane coupling agent as modifier and dispersant. *Ceram Int.* 2020;46:14583–90. <https://doi.org/10.1016/j.ceramint.2020.02.258>
58. Yang P, Sun ZF, Huang SW, Ou J, Wu SH. Digital light processing 3D printing of surface oxidized Si_3N_4 coated by silane coupling agent. *J Asian Ceram Soc.* 2022;10(1):69–82. <https://doi.org/10.1080/21870764.2021.2009096>
59. Li M, Huang HL, Wu JM, Wu YR, Shi ZA, Zhang JX, et al. Preparation and properties of Si_3N_4 ceramics via digital light processing using Si_3N_4 powder coated with $\text{Al}_2\text{O}_3\text{-Y}_2\text{O}_3$ sintering additives. *Addit Manuf.* 2022;53:102713. <https://doi.org/10.1016/j.addma.2022.102713>
60. Liu Y, Zhan LN, Wen L, Cheng L, He Y, Xu B, et al. Effects of particle size and color on photocuring performance of Si_3N_4 ceramic slurry by stereolithography. *J Eur Ceram Soc.* 2021;41:2386–94. <https://doi.org/10.1016/j.jeurceramsoc.2020.11.032>
61. Zou WJ, Yang P, Lin LF, Li YH, Wu SH. Improving cure performance of Si_3N_4 suspension with a high refractive index resin for stereolithography-based additive manufacturing. *Ceram Int.* 2022;48:12569–77. <https://doi.org/10.1016/j.ceramint.2022.01.124>

62. Cao CR, Wang C, Zhao Z. Optimization of curing behavior of Si_3N_4 UV resin for photopolymerization 3D printing. IOP Conf Ser: Mater Sci Eng. 2019;678:012013. <https://doi.org/10.1088/1757-899X/678/1/012013>
63. Rao WD, Liu Y, Cheng LJ, Liu SJ. Densification mechanism of stereolithographical dense Si_3N_4 ceramics with CeO_2 as sintering additive by field assisted sintering. J Cent South Univ. 2021;28:1233–43. <https://doi.org/10.1007/s11771-021-4631-z>
64. Altun AA, Prochaska T, Konegger T, Schwentenwein M. Dense, strong, and precise silicon nitride-based ceramic parts by lithography-based ceramic manufacturing. Appl Sci. 2020;10(3):996–1010. <https://doi.org/10.3390/app10030996>
65. Chen RF, Duan WY, Wang G, Liu BS, Zhao YT, Li S. Preparation of broadband transparent Si_3N_4 - SiO_2 ceramics by digital light processing (DLP) 3D printing technology. J Eur Ceram Soc. 2021;41:5495–504. <https://doi.org/10.1016/j.jeurceramsoc.2021.04.045>
66. Wu XQ, Xu CJ, Zhang ZM. Preparation and optimization of Si_3N_4 ceramic slurry for low-cost LCD mask stereolithography. Ceram Int. 2021;47:9400–8. <https://doi.org/10.1016/j.ceramint.2020.12.072>
67. Wu XQ, Xu CJ, Zhang ZM. Development and analysis of a high refractive index liquid phase Si_3N_4 slurry for mask stereolithography. Ceram Int. 2022;48:120–9. <https://doi.org/10.1016/j.ceramint.2021.09.087>
68. Cappi B, Ozkol E, Ebert J, Telle R. Direct inkjet printing of Si_3N_4 : characterization of ink, green bodies and microstructure. J Eur Ceram Soc. 2008;28:2625–8. <https://doi.org/10.1016/j.jeurceramsoc.2008.03.004>
69. Cappi B, Ebert J, Telle R. Rheological properties of aqueous Si_3N_4 and MoSi_2 suspensions tailor-made for direct inkjet printing. J Am Ceram Soc. 2011;94(1):111–6. <https://doi.org/10.1111/j.1551-2916.2010.04052.x>
70. Zhao ST, Xiao W, Rahaman MN, O'Brien D, Seitz-Sampson JW, Bal BS. Robocasting of silicon nitride with controllable shape and architecture for biomedical applications. Int J Appl Ceram Technol. 2017;14(2):117–27. <https://doi.org/10.1111/ijac.12633>
71. Sainz MA, Serena S, Belmonte M, Miranzo P, Osendi MI. Protein adsorption and in vitro behavior of additively manufactured 3D-silicon nitride scaffolds intended for bone tissue engineering. Mat Sci Eng C—Mater. 2020;115:110734. <https://doi.org/10.1016/j.msec.2020.110734>
72. Jin HZ, Jia DC, Yang ZH, Zhou Y. Direct ink writing of $\text{Si}_2\text{N}_2\text{O}$ porous ceramic strengthened by directional β - Si_3N_4 grains. Ceram Int. 2020;46:15709–13. <https://doi.org/10.1016/j.ceramint.2020.03.077>
73. Jiang Q, Yang DY, Yuan HY, Wang R, Hao MX, Ren WL, et al. Fabrication and properties of $\text{Si}_2\text{N}_2\text{O}$ - Si_3N_4 ceramics via direct ink writing and low-temperature sintering. Ceram Int. 2022;48:32–41. <https://doi.org/10.1016/j.ceramint.2021.08.088>
74. Clarkson CM, Wyckoff C, Parvulescu MJS, Rueschhoff LM, Dickerson MB. UV-assisted direct ink writing of Si_3N_4 /SiC preceramic polymer suspensions. J Eur Ceram Soc. 2022;42(8):3374–82. <https://doi.org/10.1016/j.jeurceramsoc.2022.03.001>
75. Agarwala MK, Bandyopadhyay A, Weeren R. van Langrana NA, Safari A, Danforth SC. Fused deposition of ceramics (FDC) for structural silicon nitride components. In: International solid freeform fabrication symposium, Austin. 1996. <http://hdl.handle.net/2152/70253>
76. Wu SX, Rangarajan S, Dai C, McCuiston R, Langrana NA, Safari A, et al. Warm isostatic pressing (WIPing) of GS44 Si_3N_4 FDC parts for defect removal. Mater Des. 2003;24:681–6. [https://doi.org/10.1016/S0261-3069\(01\)00038-3](https://doi.org/10.1016/S0261-3069(01)00038-3)
77. Rangarajan S, Qi G, Venkataraman N, Safari A, Danforth SC. Powder processing, rheology, and mechanical properties of feedstock for fused deposition of Si_3N_4 Ceramics. J Am Ceram Soc. 2000;83(7):1663–9. <https://doi.org/10.1111/j.1151-2916.2000.tb01446.x>
78. Rangarajan S, Pozsgai I, McIntosh J, McCuiston R, Harper BL, Langrana N, et al. Homogeneity, anisotropy, and texture in Si_3N_4 ceramics made by fused deposition. MRS Online Proc Lib. 1998;542:97–103. <https://doi.org/10.1557/PROC-542-97>
79. Iyer W, McIntosh J, Bandyopadhyay A, Langrana N, Safari A, Danforth SC, et al. Microstructural characterization and mechanical properties of Si_3N_4 formed by fused deposition of ceramics. Int J Appl Ceram Technol. 2008;5(2):127–37. <https://doi.org/10.1111/j.1744-7402.2008.02193.x>
80. Rabinskiy L, Ripetsky A, Sitnikov S, Solyaev Y, Kahramanov R. Fabrication of porous silicon nitride ceramics using binder jetting technology. IOP Conf Ser: Mater Sci Eng. 2016;140:012023. <https://doi.org/10.1088/1757-899X/140/1/012023>
81. Rabinskiy LN, Ripetskii AV, Pogodin VA, Sitnikov SA, Solyaev YO. Study of porous ceramic based on silicon nitride prepared using three-dimensional printing technology. Refract Ind Ceram. 2017;57:600–4. <https://doi.org/10.1007/s11148-017-0030-2>
82. Rabinskiy LN, Sitnikov SA, Pogodin VA, Ripetskiy AA, Solyaev YO. Binder jetting of Si_3N_4 ceramics with different porosity. SSP. 2017;269:37–50. <https://doi.org/10.4028/www.scientific.net/ssp.269.37>
83. Lurie SA, Solyaev YO, Rabinskiy LN, Polyakov PO, Sevostianov I. Mechanical behavior of porous Si_3N_4 ceramics manufactured with 3D printing technology. J Mater Sci. 2018;53:4796–805. <https://doi.org/10.1007/s10853-017-1881-0>
84. Xiao SS, Mei H, Han DY, Yuan WY, Cheng LF. Porous (SiC_w - Si_3N_4w)/(Si_3N_4 -SiC) composite with enhanced mechanical performance fabricated by 3D printing. Ceram Int. 2018;44:14122–7. <https://doi.org/10.1016/j.ceramint.2018.05.011>
85. Cheng ZL, Ye F, Liu YS, Qiao TL, Li JP, Qin HL, et al. Mechanical and dielectric properties of porous and wave-transparent Si_3N_4 - Si_3N_4 composite ceramics fabricated by 3D printing combined with chemical vapor infiltration. J Adv Ceram. 2019;8:399–407. <https://doi.org/10.1007/s40145-019-0322-8>
86. Li XM, Zhang LT, Yin XW. Microstructure and mechanical properties of three porous Si_3N_4 ceramics fabricated by different techniques. Mat Sci Eng A—Struct. 2012;549(15):43–9. <https://doi.org/10.1016/j.msea.2012.03.114>
87. Li XM, Zhang LT, Yin XW. Effect of chemical vapor infiltration of Si_3N_4 on the mechanical and dielectric properties of porous Si_3N_4 ceramic fabricated by a technique combining 3-D printing and pressureless sintering. Scr Mater. 2012;67(4):380–3. <https://doi.org/10.1016/j.scriptamat.2012.05.030>
88. Duan WY, Yin XW, Cao FX, Jia YL, Xie Y, Greil P, et al. Absorption properties of twinned SiC nanowires reinforced Si_3N_4 composites fabricated by 3D-printing. Mater Lett. 2015;159:257–60. <https://doi.org/10.1016/j.matlet.2015.06.106>

89. Duan WY, Fan Z, Wang H, Zhang JY, Qiao TL, Yin XW. Electromagnetic interference shielding and mechanical properties of Si_3N_4 -SiOC composites fabricated by 3D-printing combined with polymer infiltration and pyrolysis. *J Mater Res.* 2017;32(17):3394–401. <https://doi.org/10.1557/jmr.2017.150>
90. Rodrigues SJ, Chartoff RP, Klosterman DA, Agarwala M, Hecht N. Solid freeform fabrication of functional silicon nitride ceramics by laminated object manufacturing. In: International solid freeform fabrication symposium, Austin. 2000. <https://doi.org/10.26153/tsw/2052>
91. Liu SC, Ye F, Liu LM, Liu Q. Feasibility of preparing of silicon nitride ceramics components by aqueous tape casting in combination with laminated object manufacturing. *Mater Des.* 2015;66:331–5. <https://doi.org/10.1016/j.matdes.2014.10.079>
92. Park DS, Cho BW. Fabrication of a complex-shaped silicon nitride part with aligned whisker seeds using LOM technique. *J Korean Ceram Soc.* 2003;40(10):931–5. <https://doi.org/10.4191/KCERS.2003.40.10.931>
93. Zhang JX, Ye F, Jiang DL, Iwasa M. Preparation of bulk Si_3N_4 from tape casting and lamination. *Ceram Int.* 2006;32:277–82. <https://doi.org/10.1016/j.ceramint.2005.03.003>
94. Pope MJ, Patterson MCL, Zimbeck W, Fehrenbacher M. Laminated object manufacturing of Si_3N_4 with enhanced properties. In: International solid freeform fabrication symposium, Austin. 1997. <http://hdl.handle.net/2152/71431>
95. Olakanmi EO, Cochrane RF, Dalgarno KW. A review on selective laser sintering/melting (SLS/SLM) of aluminium alloy powders: processing, microstructure, and properties. *Prog Mater Sci.* 2015;74:401–77. <https://doi.org/10.1016/j.pmatsci.2015.03.002>
96. Fan ZQ, Zhao YT, Tan QY, Mo N, Zhang MX, Lu MY, et al. Nanostructured Al_2O_3 -YAG-ZrO₂ ternary eutectic components prepared by laser engineered net shaping. *Acta Mater.* 2019;170:24–37. <https://doi.org/10.1016/j.actamat.2019.03.020>
97. Boegelein T, Dryepondt SN, Pandey A, Dawson K, Tatlock GJ. Mechanical response and deformation mechanisms of ferritic oxide dispersion strengthened steel structures produced by selective laser melting. *Acta Mater.* 2015;87:201–15. <https://doi.org/10.1016/j.actamat.2014.12.047>
98. Huang JG, Qin Q, Wang J. A review of stereolithography: processes and systems. *Processes.* 2020;8(9):1138. <https://doi.org/10.3390/pr8091138>
99. Quan HY, Zhang T, Xu H, Luo S, Nie J, Zhu XQ. Photocuring 3D printing technique and its challenges. *Bioact Mater.* 2020;5:110–5. <https://doi.org/10.1016/j.bioactmat.2019.12.003>
100. He RJ, Zhou NP, Zhang KQ, Zhang XQ, Zhang L, Wang WQ, et al. Progress and challenges towards additive manufacturing of SiC ceramic. *J Adv Ceram.* 2021;10(4):637–74. <https://doi.org/10.1007/s40145-021-0484-z>
101. Ziaeem M, Crane NB. Binder jetting: a review of process, materials, and methods. *Addit Manuf.* 2019;28:781–801. <https://doi.org/10.1016/j.addma.2019.05.031>
102. Bhushan B, Caspers M. An overview of additive manufacturing (3D printing) for microfabrication. *Microsyst Technol.* 2017;23:1117–24. <https://doi.org/10.1007/s00542-017-3342-8>
103. Diener S, Franchin G, Achilles N, Kuhnt T, Rosler F, Katsikis N, et al. X-ray microtomography investigations on the residual pore structure in silicon nitride bars manufactured by direct ink writing using different printing patterns. *Open Ceram.* 2021;5:100042. <https://doi.org/10.1016/j.oceram.2020.100042>
104. Wang WQ, Zhang L, Dong XJ, Wu JQ, Zhou Q, Li SW, et al. Additive manufacturing of fiber reinforced ceramic matrix composites: advances, challenges, and prospects. *Ceram Int.* 2022;48:19542–56. <https://doi.org/10.1016/j.ceramint.2022.04.146>
105. Zhang XQ, Zhang KQ, Zhang B, Li Y, He RJ. Quasi-static and dynamic mechanical properties of additively manufactured Al_2O_3 ceramic lattice structures: effects of structural configuration. *Virtual Phys Prototy.* 2022;17(3):528–42. <https://doi.org/10.1080/17452759.2022.2048340>
106. Zhang XQ, Zhang KQ, Zhang L, Wang WQ, Li Y, He RJ. Additive manufacturing of cellular ceramic structures: from structure to structure-function integration. *Mater Des.* 2022;215:110470. <https://doi.org/10.1016/j.matdes.2022.110470>

How to cite this article: Dong X, Wu J, Yu H, Zhou Q, Wang W, Zhang X, et al. Additive manufacturing of silicon nitride ceramics: A review of advances and perspectives. *Int J Appl Ceram Technol.* 2022;19:2929–2949.
<https://doi.org/10.1111/ijac.14162>